

Structural Integrity of Polymer Matrix Composites Exposed to Fire Conditions

By

John Vincent Bausano

Thesis submitted to the Faculty of the
Virginia Polytechnic Institute and State University
in partial fulfillment of the requirements for the degree of

Master of Science
in
Engineering Mechanics

Approvals

John J. Lesko, Chair

Scott W. Case

Committee Chairman

Committee Member

Judy S. Riffle

Committee Member

Tuesday, January 7, 2003

Blacksburg, Virginia

Keywords: Composites, Fire, Thermal and Mechanical Loading, Failure Times

Structural Integrity of Polymer Matrix Composites Exposed to Fire Conditions

John Vincent Bausano

(Abstract)

Polymer matrix composites (PMC's) perform well under many loading conditions and situations. Exposure of PMC's to fire is a concern due to their inherent material degradation at elevated temperatures. The elevated temperature response of PMC's to combined thermal and mechanical loads are especially of concern.

PMC thermal and mechanical properties undergo transformations at elevated temperatures. Some of these effects are reversible if the maximum temperatures are lower than approximately 200°C. The stiffness is significantly reduced at elevated temperatures but if the applied temperature is under the thermal degradation temperature of the matrix, the stiffness should be recoverable upon cooling. Some effects like the endothermic decomposition of the matrix are not reversible effects.

This study focuses on reversible properties in the temperature range from room temperature to about 200°C. Thermally these effects alter the thermal conductivity and specific heat. Reversible elastic effects considered are the off axis stiffness reductions as functions of temperatures.

Thermal profile predictions were conducted using a finite difference code that included convection and radiation effects on the front and back faces of the composite. These predictions were shown to be in good agreement with experimental data.

A modified classic laminate analysis (CLT) was implemented to predict the failure times of the composites under combined thermal and mechanical loading. The Budiansky-Fleck micro-buckling analysis technique was used as the failure function of the [0°] surface plies. A finite element analysis (FEA) analysis was also performed and showed good agreement with the experimental data.

Acknowledgments

I would like to give thanks to the following people for their support in conjunction with this work.

My Committee Members:

- Dr. Jack Lesko: Thank you for giving me the opportunity to be a part of the MRG group. You have been an advisor, mentor and friend through the years.
- Dr. Scott Case: If I ever came to you with a question you seemed to answer it every time, but give me TWO new questions to think about.
- Dr. Judy Riffle: The guidance you provided me throughout this research has been invaluable, thank you very much.

Materials Response Group Members:

- Beverly Williams: Thank you so much for making everything work smoothly around the MRG. Without you none of us would get a thing done.
- Mac McCord: Without your ingenious lab setups I would have never completed one experiment. Thank you for taking care of me in the labs.
- Michael Hayes: You gave me tons of good advice, but most importantly you were always ready for lunch, and a game of basketball.
- Tozer Bandorawalla: I always came to you when I was stuck with something and you would show me the error of my ways. Thanks for all the help.
- Howard Halverson: Thank you for showing me the ropes with ANSYS. I know it was hard putting up with my incessant questions but everyone knows you are a better reference than the ANSYS manual itself.
- Tim Schniepp: Timmy, thanks for coming to VT with me from Winona. I had a great time with you these last few years.

Table of Contents:

List of Figures: vii

List of Tables: ix

CHAPTER 1 Introduction and Background 1

 1.1 Introduction..... 1

 1.2 Composite Phenomena at Elevated Temperatures..... 2

 1.2.1 Smoke and Combustion Gas Generation 2

 1.2.2 Heat Release & Ignitability..... 3

 1.2.3 Fire Growth..... 3

 1.2.4 Mass Loss & Charring 4

 1.2.5 Delamination..... 5

 1.2.6 Material Property Evolution 5

 1.3 Previous Modeling Efforts..... 5

 1.4 Research Goals..... 9

 1.5 Figures..... 10

CHAPTER 2 Experimental Procedures 11

 2.1 Experimental Overview 11

 2.2 Description of Materials 11

 2.2.1 Dow Momentum 411 350/Fiberglass Composite 11

 2.2.2 Phenolic Epoxy/Carbon Fiber..... 11

 2.3 Specific Heat..... 12

 2.3.1 Test Motivation..... 12

 2.3.2 Test Description 12

 2.4 Thermal Diffusivity 13

 2.4.1 Test Motivation..... 13

 2.4.2 Test Description 13

 2.5 Off Axis Stiffness Reduction 14

 2.5.1 Test Motivation..... 14

 2.5.2 Test Description 14

 2.6 Combined Thermal & Compressive Loading..... 14

 2.6.1 Test Motivation..... 14

2.6.2	Test Description	15
2.7	Figures.....	16
CHAPTER 3	Experimental Results.....	18
3.1	Specific Heat.....	18
3.1.1	Acquired Data.....	18
3.1.2	Observations and Remarks	18
3.2	Thermal Diffusivity	18
3.2.1	Acquired Data.....	18
3.2.2	Observations and Remarks	19
3.3	Off Axis Stiffness Reduction.....	19
3.3.1	Acquired Data.....	19
3.3.2	Observations and Remarks	20
3.4	Combined Thermal & Compressive Loading.....	20
3.4.1	Acquired Data.....	20
3.4.2	Observations and Remarks	22
3.5	Figures.....	25
CHAPTER 4	Analytical Development and Simulations	40
4.1	Thermal Profile Models	40
4.1.1	Introduction.....	40
4.1.2	Boundary Conditions	40
4.2	Thermal Model Development.....	41
4.2.1	Finite Difference	41
4.2.2	Finite Element.....	43
4.3	Mechanical Models.....	44
4.3.1	Introduction.....	44
4.3.2	Temperature Profiles Used	44
4.3.3	Mechanical Material Properties as a Function of Temperature	44
4.3.4	Modified CLT	45
4.3.5	Mechanical Finite Element Analysis	45
4.3.6	Budiansky and Fleck Failure Criteria	46
4.4	Figures.....	48

CHAPTER 5	Analytical Results Compared to Experimental Data	53
5.1	Laminate Thermal Response.....	53
5.1.1	Finite Difference Temperature Results and Comparisons	53
5.2	Mechanical Responses	54
5.2.1	Time to Failure Predictions.....	54
5.2.2	Strain Profile Predictions	55
5.3	Figures.....	56
CHAPTER 6	Conclusions and Recommendations	64
6.1	Conclusions.....	64
6.1.1	Thermal	64
6.1.2	Mechanical	65
6.2	Recommendations for Future Work.....	65

List of Figures:

Figure 1-1: Combustion Process: Heat and Mass Transfers	10
Figure 2-1: Combined Thermal Mechanical Loading Setup	16
Figure 2-2: Experimental Setup	17
Figure 3-1: Specific Heat of Glass/Vinyl-Ester Composite.....	25
Figure 3-2: Specific Heat of Carbon/Phenolic-Epoxy Composite.....	25
Figure 3-3: Thermal Diffusivity of Carbon/Phenolic-Epoxy Composite	26
Figure 3-4: Thermal Diffusivity of Carbon/Phenolic-Epoxy Normalized to 21°C.....	26
Figure 3-5: Thermal Diffusivity of Glass/Vinyl-Ester Composite	27
Figure 3-6: Stiffness Reduction Normalized to Room Temperature Value	27
Figure 3-7: Scaled E_{22} Reduction Curves	28
Figure 3-8: Example Test, Recorded % Strain, Front & Back Temperatures	28
Figure 3-9: 5 [kW/m ²] Temperature Profiles.....	29
Figure 3-10: 10 [kW/m ²] Temperature Profiles.....	29
Figure 3-11: 15 [kW/m ²] Temperature Profiles.....	30
Figure 3-12: 20 [kW/m ²] Temperature Profiles.....	30
Figure 3-13: Average Temperature Comparison for All Heat Fluxes	31
Figure 3-14: 5 [kW/m ²] Strain Profiles.....	31
Figure 3-15: 10 [kW/m ²] Strain Profiles.....	32
Figure 3-16: 15 [kW/m ²] Strain Profiles.....	32
Figure 3-17: 20 [kW/m ²] Strain Profiles.....	33
Figure 3-18: 5 [kW/m ²] Maximum Strain Shifts	33
Figure 3-19: 10 [kW/m ²] Maximum Strain Shifts	34
Figure 3-20: 15 [kW/m ²] Maximum Strain Shifts	34
Figure 3-21: 20 [kW/m ²] Maximum Strain Shifts	35
Figure 3-22: 5 [kW/m ²] Change in % Strain Slope	35
Figure 3-23: 10 [kW/m ²] Change in % Strain Slope	36
Figure 3-24: 15 [kW/m ²] Change in % Strain Slope	36
Figure 3-25: 20 [kW/m ²] Change in % Strain Slope	37
Figure 3-26: Initial Strain rate vs. Applied Heat flux	37
Figure 3-27: Times-To-Failure under Combined Loading	38

Figure 3-28: [0°] Ply Alignment Before and After Kinking	38
Figure 3-29: Compressive Failure Modes.....	39
Figure 4-1: Simulation flow chart.....	48
Figure 4-2: FEA Model.....	49
Figure 4-3: Budiansky & Fleck Kink Band Schematic	49
Figure 4-4: Shear Stress – Strain Properties of Glass/Vinyl Ester [+/-45°] Laminates	50
Figure 4-5: Shear Moduli of Glass/Vinyl Ester [+/-45°] Laminates	50
Figure 4-6: Shear Yield Properties	51
Figure 4-7: Budiansky-Fleck Compression Strength vs. Temperature.....	51
Figure 4-8: Normalized Shear Modulus and Compression Strength vs. Temperature.....	52
Figure 5-1: 5 kW/m ² Temperature Profile Results vs. Collected Data.....	56
Figure 5-2: 10 kW/m ² Temperature Profile Results vs. Collected Data.....	56
Figure 5-3: 15 kW/m ² Temperature Profile Results vs. Collected Data.....	57
Figure 5-4: 20 kW/m ² Temperature Profile Results vs. Collected Data.....	57
Figure 5-5: Through the Thickness Temperature Perditions	58
Figure 5-6: 20 kW/m ² Time to Failure Predictions	59
Figure 5-7: 15 kW/m ² Time to Failure Predictions	59
Figure 5-8: 10 kW/m ² Time to Failure Predictions	60
Figure 5-9: 5 kW/m ² Time to Failure Predictions	60
Figure 5-10: 5 kW/m ² /44.8 MPa Strain Profile Predictions vs. Experimental Data.....	61
Figure 5-11: 10 kW/m ² /27.6 MPa Strain Profile Predictions vs. Experimental Data.....	61
Figure 5-12: 15 kW/m ² /27.6 MPa Strain Profile Predictions vs. Experimental Data.....	62
Figure 5-13: 20 kW/m ² /13.8 MPa Strain Profile Predictions vs. Experimental Data.....	62
Figure 5-14: FEA Deformation Prediction	63

List of Tables:

Table 2-1: Glass/Dow 411 350 Room Temperature 0° Ply Properties 11

Table 2-2: Carbon/Phenolic-Epoxy Room Temperature [0°] 6 Ply Properties..... 12

Table 2-3: Carbon/Phenolic-Epoxy Room Temperature [90°/0°] 3s Laminate Properties 12

Table 3-1: Carbon/Phenolic-Epoxy Thermal Diffusivity 19

Table 4-1: Finite Difference Convection Coefficients..... 41

CHAPTER 1 Introduction and Background

1.1 Introduction

Polymer matrix composite (PMC) materials are lightweight, durable, and cost effective material solutions for a variety of applications ranging from high performance military designs to consumable goods. While the high strength to weight ratios lend themselves to PMC solutions in the aeronautics community, the durability and life cycle cost benefits are enabling the use of PMC's in other fields. Over time the use of PMC's has broadened from the traditional military applications of aircrafts, rockets and satellites into new areas such as civil infrastructure. Civil infrastructures utilizing PMC's include new bridge decks, as well as rehabilitated structures.

The implementation of PMC's is still inhibited in some applications due to their performance in fire conditions. The polymer matrix of the PMC undergoes significant physical, chemical and mechanical changes during exposure to fire. This reality prohibits further use of PMC's in many applications.

Fire produces complex effects on PMC's, which have been investigated for over 20 years. The thermal response of a composite to fire scenarios is a complex coupled process [1] characterized by energy feedback from a flame to the PMC's surface and the subsequent gasification of the PMC to form combustible byproducts. The gasification of the solid phase and the combustion of the gaseous phase exhibit complex coupled chemical reactions and involve heat and mass transfer processes as depicted in Figure 1-1. At sufficient temperatures combustible products are transported from the solid phase to the gaseous phase. The gas phase transfers a small amount of the heat generated during the gas phase oxidation reactions back to the material surface.

The thermal response must first be characterized in order to explain the mechanical phenomena because of the dependence of mechanical properties on temperature. Significant work has been done on predicting of the thermal profiles of these composites exposed to heat sources. Much less work in the area of the mechanics of PMC's at elevated temperatures has been pursued. Further investigations of mechanical properties change at elevated temperatures must be undertaken before any significant modeling or predictions can be done. There also exists an incomplete understanding of failure modes and mechanisms that control PMC's failures at elevated temperatures which must further investigated.

This work is intended to be a first step towards a complete, simultaneous thermal and mechanical loading analysis technique. This will, ultimately, also account for reversible lower temperature effects combined with permanent higher temperature material degradation effects. The lower temperature phenomena must first be identified and modeled before further effects are included in the analysis.

1.2 Composite Phenomena at Elevated Temperatures

PMC's have long been used in a variety of different environments with great success. However, new applications that require the material to be exposed to high temperatures introduce some concerns. Composites exposed to elevated temperatures will undergo both reversible and irreversible transformations. Elevated temperatures can have many effects on the polymer matrix of the composite. The fibers are generally considered to be unaffected by high temperatures. The following sections are intended to provide a description of some phenomena affecting PMC's at elevated temperatures.

1.2.1 Smoke and Combustion Gas Generation

During a fire, life is at risk due to direct contact with fire and also from exposure to gaseous byproducts. The smoke produced during burning of PMC's can be more of a concern to people in the vicinity of the fire than the fire itself. In fact most deaths in fires are caused by carbon monoxide inhalation. Both the toxicity and the smoke density are issues. If the smoke becomes too dense, firefighters will be unable to adequately fight the fire and the ability of people to escape the fire will be hindered. If the smoke is toxic there is an obvious health concern to all people exposed.

A common test method to characterize the degree of smoke generation, or smoke obscuration, is ASTM E 662. The test is conducted in a closed chamber and the light attenuation is recorded. The sample is subjected to a radiant heat flux of 25 kW/m^2 , under both piloted ignition and smothering conditions. The resulting light transmissions provide specific optical density (Ds).

“Combustion gas generation” is defined as the gases produced by a combusting material. Carbon monoxide and carbon dioxide and the most prevalent combustion gases HCl, HCN and others may also evolve depending on the chemistry of the matrix material. If a matrix is

halogenated, as in a brominated vinyl ester or epoxy, hydrogen bromide can also be a combustion byproduct. ASTM E 1354 is the commonly used standard to determine the quantities of these combustion gases. Significant research has been conducted on classification of smoke density and combustion gas concentration of various matrix materials by Sorathia et al. [2-4] for the U.S. Navy.

1.2.2 Heat Release & Ignitability

The heat release rate (HHR) is defined as the amount of heat generated in a fire due to the combustion of a material. Combustion reactions that are exothermic include reactions that generate carbon monoxide, carbon dioxide and the consumption of oxygen [5]. Ignitability is the time required for a material to reach flaming combustion.

ASTM E 1354 (Oxygen Consumption Cone Calorimeter) is the standard test for determining the HHR and ignitability. In this test a small sample is placed horizontally relative to a cone heating element and exposed to controlled amounts of radiant energy. Samples are typically exposed to 25, 50, 75 or 100 kW/m², and these heat fluxes are thought to represent a small fire, large trash can fire, a large fire and a fully developed oil fire. This test can be used to determine the HHR, ignitability, mass loss rates and effective heat of combustion. The test utilizes the oxygen consumption principle [6] in which HHR is calculated from oxygen depletion in the gas flow.

The HHR and the peak HHR are primary parameters determining the size and growth characteristics of a fire. Sorathia and numerous other authors [7-10] have collected and produced a large amount of data characterizing the flammability of a variety of polymers and composites.

1.2.3 Fire Growth

Fire growth or flamespread tests characterize the speed at which a flame spreads. There are a variety of tests to determine the degree a flame spreads. Examples are, ASTM E 84 (Tunnel Test), ASTM E 1354 (Cone Calorimeter), ASTM E 1321 (Lateral Ignition and Flamespread) and UL 94 (Oxygen Index). The tests range from small lab scale tests (ASTM E 1354) to full scale tests (ASTM E 1321).

The HHR is the most important factor in the spread of fire. If the energy released by the combustion process is sufficient, the fire will grow and spread instead of self extinguish. ASTM

E 1354 determines HHR, among other things. ASTM E 1321 is a full scale version of ASTM E 1354. The test consists of constructing a vertical 90° corner of the material and placing it in a large scale cone calorimeter. An ignition source, usually a gas burner, of specified heat flux output is used to ignite the material at the bottom of the corner. Wall temperatures and flamespread speeds are recorded along with usual cone calorimetry data. Ohlemiller [11, 12] and Sorathia [3] have conducted several studies on a variety of composite materials including brominated and non-brominated vinyl-ester composites in an effort to characterize the vertical flamespread phenomena.

1.2.4 Mass Loss & Charring

PMC's at elevated temperatures begin to lose mass as the polymer matrix undergoes chemical changes. At elevated temperatures thermal degradation reactions occur, producing small amounts of gaseous byproducts. The majority of evolved gases from polymers are combustible. Depending on the specific polymer the thermal degradation reaction can vary. Several authors have studied the thermal degradation chemistry of polymers [13-15].

Char can be defined as carbonized polymer residue which remains in the solid phase. The formation of char is generally recognized as a mechanism for reducing flammability [4]. Char formation reduces the amount of volatile gaseous products available for gas phase consumption. That is, the production of char limits the amount of gaseous fuel for combustion and hence lowers the levels of heat transferred from the flame to the surface of the solid phase. This lowers the surface temperatures, and reduces rates of degradation reactions. The thermal conductivity of char is low; and a layer of char functions as insulation for the remaining underlying polymer.

Thermogravimetric Analysis (TGA) is a widely used thermal analysis technique for characterizing the thermal performance of polymers. The technique consists of placing a small sample of material, usually a few milligrams, in an inert pan connected to a balance. The test can be conducted in an inert atmosphere like N₂ or air. The sample is exposed to heat under either isothermal or dynamic conditions and the change in mass is recorded. Mass loss kinetics can be determined from such experiments along with char yields.

1.2.5 Delamination

Delamination of PMC laminates can be induced by fire conditions. Delamination is defined as the mechanical separation of inter-laminar layers or plies. Sources of delamination can be attributed to internal pressure build up resulting from expansion of hot gases. These gases consist of combustion gases, i.e. combustion byproducts, and evolution of absorbed water or other liquids (e.g. residual solvents or low molecular weight components in the matrix). Because of the rapid heating conditions of fires the hot gases are incapable of quickly diffusing through the matrix material, thus producing a pressure build up. Due to this fact initial moisture content is a major factor in the development of delaminations in thick composites exposed to fire [16, 17].

1.2.6 Material Property Evolution

Most materials exhibit changes in thermal and mechanical properties as a function of temperature. Aluminum for example undergoes significant strength loss around 300°C. Temperature effects on PMC's mechanical properties. It has been shown [2] that glass/vinyl ester composites lose up to 50% of their room temperature stiffness at 120°C. The strength of other PMC's also suffers similar losses at elevated temperatures. Thermal properties can also evolve or change as a function of temperature. Specific heat and thermal conductivity both have been shown to change as a function of temperature [16]. Some properties like stiffness also depend on the combination of temperature, time (creep), and load. It is clear that for any accurate thermal or mechanical simulations that almost all properties must be at least a function of temperature.

1.3 Previous Modeling Efforts

The first attempts at the modeling of composites exposed to fire conditions were performed over 20 years ago [18]. Modeling efforts have focused on predictions of temperature profiles. Some work has been done in the area of mechanical response predictions, and a few investigations have been performed on combined thermal and mechanical loading of composites. Research has been conducted that predicts residual mechanical properties of composites that have been exposed to elevated temperatures and then allowed to cool. Composites are weaker and less stiff at elevated temperatures, so this suggests that the critical state of interest is when

the composites are hot and under load. Furthermore, composite tensile properties are dominated by the fiber reinforcement, while compressive properties are a matrix dominated response. This indicates that the compressive properties of composites are more critically affected by elevated temperatures. Further investigations are required to predict the effects of combined thermal and compressive mechanical loading on composite laminates.

One of the first studies of residual mechanical strengths of PMC's after exposure to intense heating was conducted by Pering [18] in 1980. Samples were exposed to intense heat for specified durations of time and the mass loss and strength were recorded. Some correlations between the observed mass loss and strength loss were observed. There was no attempt at modeling these phenomena.

Griffis et al. [19] were the first to present a thermal response model predicting the temperature profiles of composites exposed to external heating. A one – dimensional finite difference code was developed that predicted the temperature distributions through an AS/3501 graphite/epoxy composite irradiated with a laser. The model accounted for fiber ablation, and matrix decomposition. The boundary conditions were represented as convection and radiation boundaries. The predicted temperatures as well as the mass loss were in good agreement with experimental data. The boundary conditions used were idealized, steady state and uniform heat fluxes, which does not adequately represent a fire situation.

A few years later (1985) Chen et al. [20] built upon the model developed by Griffis et al. [19] to would analyze the combined effects of thermal and mechanical loading. A finite element code was developed that predicted the resulting strains of a combined loading situation. Coupling the finite element analysis with the maximum stress failure criteria enabled predictions of the time to failure of composites loaded in tension and subjected to laser heating. As with [19] the thermal profile predictions agreed well with experiment. However, the times to failure were an order of magnitude off from experimental data.

In 1986 Griffis et al. [21] expanded on their previous work and the work of Chen et al. The same thermal and mechanical models were implemented. The Tsai-Wu failure criterion was compared to predictions of the maximum stress criterion. Again the thermal model predictions compared well to experimental data. However the times to failure predictions of the tension loaded specimens irradiated by a laser were lacking for both failure criteria considered.

A year later Henderson [22] attempted to improve the thermal response model utilized in [19-21]. Although the previous thermal model correlated well with data it was lacking some fundamental governing physics. This model was a one-dimensional representation of the transient heating process. It included the endothermic decomposition of matrix material, evolution of pyrolysis gases, and storage and mass transfer of these gases. This model's predictions compared quite well to the experimental data over large time and temperature regions, up to 600 seconds and 800°C. This thermal model was never employed in conjunction with a mechanical prediction model.

Milke [23] furthered the work on temperature predictions. The model was a three-dimensional thermal response model for anisotropic composite laminates. The boundary conditions were non-uniform radiative and convective heat fluxes. This model also did not account for the mass loss or endothermic decomposition of materials. The predicted temperature profiles were in good agreement with experimental data.

In 1992 McManus [16, 17] developed models for thermal and mechanical response of carbon phenolic composites exposed to rapid heating. The thermal model is one of the most complete representations of the physics to date. The model considered the formation of a char layer, mass loss, vapor (water) and volatile formation along with diffusion of the gases through the thickness. The mechanical model was based on the equations of three dimensional elasticity, and was able to predict the number and depth of delaminations along longitudinal, transverse and interlaminar stresses. The internal pressure build up do to the expansion of trapped gases is also calculated. The temperature profiles agreed with experimental data very well, as did the depth and number of induced delaminations. This model was never used in a larger structural analysis or combined loading investigation.

Also in 1992 Sullivan [24, 25] introduced a finite element method modeling the thermo-chemical decomposition and mechanical response of composites, it was hypothesized that the response of composites was directly related to the diffusion and pressures of gases produced during chemical decomposition. A thermal response model was not developed. The mechanical model required temperature profiles from experiments as input. Two tests were conducted to validate the code. The first was a thermal strain growth experiment. This consisted of clamping only one end of a cylindrical sample and applying a uniform heat, while recording the induced strain. The second test clamped both ends of the sample and restricted it from expanding, and

the loads required to achieve this were recorded. The modeling results of both experiments were acceptable, but no further investigations to obtain failure predictions were done and the thermal boundary conditions were idealized.

Gibson [26] developed a thermal response model similar to previous models in 1994. This was a one-dimensional model that included effects due to endothermic matrix decomposition, and volatile gas convection. A limited amount of experimental data was presented to validate the model. This thermal model was also never used as input to a mechanical response model.

McManus and Chamis [27] developed a model that predicted the stresses and amount of damage (mass loss) induced in composites exposed to elevated isothermal temperatures. An empirical model was produced that correlated the effects of mass loss and crosslinking to the deterioration of mechanical properties and dimensional changes. Matrix shrinkage due to mass loss is translated through micromechanical principles into resulting ply property evolution. The predicted loss in mass and flexural strength of isothermally aged samples correlates well with the limited amount of experimental data. Further validation should be conducted.

Sorathia [2], in 1997, reported effects of isothermal aging on the moduli of a range of composite materials. No modeling efforts were done but large amounts of data were collected. Dynamic thermal mechanical analysis (DTMA) showed that the residual stiffness of a glass vinyl ester composite exposed to isothermal aging at temperatures above 200°C had significant damage.

Another thermal and mechanical model was developed by Tuttle et al. [28] in 1997. This thermal model was a one-dimensional heat transfer code that predicted “through the thickness” temperature distributions for an input uniform heat flux. The thermal model did take into account pyrolysis effects but did not consider transport of these gases through the material. The mechanical code was based on classic laminate theory (CLT), where both elastic and visco-elastic effects are considered. An example analysis was presented but no experimental validation was attempted.

Dodds et al. [29] developed one of the most recent thermal response models. This model was similar to previous finite difference codes that accounted for the endothermic decomposition of the matrix and the convection of pyrolysis gases. A TGA analysis was conducted to determine the matrix mass loss kinetics. The boundary conditions of this model were simple,

uniform – steady state heat flux. The resulting predictions correlated well with the experimental data, but again no mechanical response model, or combined loading effects were considered.

1.4 Research Goals

The goal of this research was to develop a thermo-mechanical modeling technique that could be used to predict mechanical performance of composite materials subjected to simulated fire conditions and mechanical loads simultaneously. Material characterization was required to determine thermal properties as a function of temperature. Characterization of the thermal properties specific heat and thermal conductivity were determined experimentally for vinyl ester - glass composite material system. Thermal and mechanical modeling of the composite will be presented. Because of the previous research in the area of thermal predictions i.e. temperature distributions throughout a composite, the emphasis of the presented research will be on the combined thermal and mechanical loading conditions. The strain profiles and times to failure of combined loaded samples will be presented and compared to experimental data. This analysis will focus only on the temperature regime from room temperature to 200°C. Developing a complete understanding of the phenomena at these temperatures will provide the foundation for continued work which will include both reversible and irreversible effects including char formation, mass loss and visco-elastic effects.

1.5 Figures

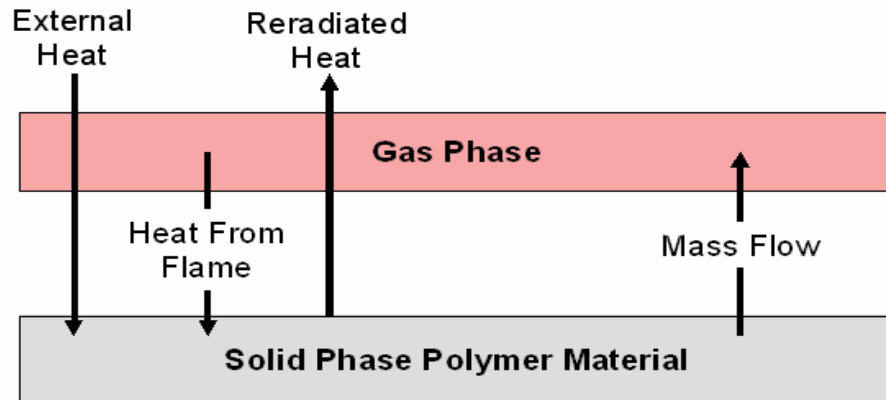


Figure 1-1: Combustion Process: Heat and Mass Transfers

CHAPTER 2 Experimental Procedures

2.1 Experimental Overview

The following section provides a description of experimental test motivations and descriptions. Experiments were conducted in an effort to accurately determine thermal and mechanical properties as a function of temperature. Experiments were performed on two material systems, a glass/vinyl ester and carbon/phenolic-epoxy composite. Not all tests were run on both material systems. This was due to the limitations of some of the testing techniques.

2.2 Description of Materials

2.2.1 Dow Momentum 411 350/Fiberglass Composite

One of the material systems was a quasi-isotropic vinyl ester/fiberglass composite. The resin matrix was a commercially available Dow Derakane Momentum 411-350, which is an epoxy vinyl ester resin. The resin had a styrene content of 20% and was loaded with ASP 400 filler at a level of 20 parts by weight. The fiberglass reinforcement was Owens Corning E-glass. The laminates were manufactured via pultrusion. The fiber orientation of the laminates were $[0^\circ, 90^\circ, \pm 45^\circ, 90^\circ]_S$, with an approximate fiber volume fraction of 63%. The geometry profile of the pultrusion die was 4 mm thick by 180 mm wide. Previously Phifer [30] estimated the room temperature ply level properties of a similar pultruded laminate Table 2-1. Laminate compression strength was determined to be 161 E+6 Pa.

Table 2-1: Glass/Dow 411 350 Room Temperature 0° Ply Properties

E_{11} [Pa]	E_{22} [Pa]	G_{12} [Pa]	ν_{12}	α_{11} [$\mu \epsilon/^\circ\text{C}$]	α_{22} [$\mu \epsilon/^\circ\text{C}$]
355 E+9	14.2 E+6	5.0 E+9	0.283	7.7	36.0

2.2.2 Phenolic Epoxy/Carbon Fiber

The second material tested was a phenolic-epoxy/carbon fiber composite. This resin was a new system that was developed at Virginia Tech by Dr. Riffle et al. [31]. The resin is a 65/35 weight/weight blend of phenolic novolac with an average functionality of 7-1 to epoxy. This ratio was chosen on the basis that it exhibited a unique combination of both properties derived from the epoxy and phenolic resins. The matrix exhibited high toughness and was void free. It

retained much of the flame retardance characteristics of phenolic networks while still maintaining its processability. The reinforcing fiber was carbon AS4-GP; the approximate fiber volume fraction for this material system was 57%. These laminates were manufactured by a melt pre-prepreg followed by a standard autoclave technique. Tensile laminate properties are listed in Table 2-2 and Table 2-3 for a six ply unidirectional lay-up and a 12 ply [90°/0°] lay-up.

Table 2-2: Carbon/Phenolic-Epoxy Room Temperature [0°] 6 Ply Properties

E_{11} (Pa)	X_{11} (Pa)	ν_{12}
129 E+9	1.93 E+9	0.234

Table 2-3: Carbon/Phenolic-Epoxy Room Temperature [90°/0°] 3s Laminate Properties

E_{11} (Pa)	X_{11} (Pa)
70.3 E+9	1.02 E+9

2.3 Specific Heat

2.3.1 Test Motivation

The specific heat or heat capacity is the quantity of heat per unit mass required to raise the temperature of a material one degree. This quantity is an important parameter in the heat equation. The simple one-dimensional form of the heat equation is given in Equation (2-1).

$$\frac{\partial T}{\partial t} = \frac{k}{\rho c_p} \frac{\partial^2 T}{\partial x^2} \quad (2-1)$$

T , t , k , ρ and c_p are the temperature, time, thermal conductivity, density, and specific heat respectively. As the temperature in the material is increased the thermal properties will change. Hence for an accurate description these quantities must be determined as a function of temperature.

2.3.2 Test Description

The tests were performed on a TA Q100 DSC, which implements “T-zero” technology. This increases the sensitivity of the instrument and eliminates the need to determine baselines before every experiment. The test method followed was ASTM E-1269-01. Both materials were tested, and the samples analyzed were approximately 5 milligrams. Each sample was subjected to a temperature ramp from room temperature to 300°C at 5°C/min. Nitrogen was used as the

purge gas to minimize degradation. The resulting output of the test was a continuous curve of specific heat versus temperature.

2.4 Thermal Diffusivity

2.4.1 Test Motivation

Not only is the specific heat required for the modeling of the thermal response of a material, so are the thermal conductivity and density. Instruments were not available for measuring thermal conductivity directly. Thus thermal diffusivity was determined experimentally and thermal conductivity was calculated by the relationship in Equation (2-2). The thermal diffusivity (α) is defined as the thermal conductivity (k) divided by the product of density (ρ) and specific heat (c_p).

$$\alpha = \frac{k}{c_p \cdot \rho} \quad (2-2)$$

All four parameters must be determined in Equation (2-2). Three of the four parameters are experimentally determined (α , c_p , ρ) and the last (k) was calculated through rearrangement of terms.

2.4.2 Test Description

The thermal diffusivity test was performed in accordance with ASTM E 1461 – 01, “Standard Test Method for Thermal Diffusivity by the Flash Method.” Two instruments were used to determine the thermal diffusivity at a range of temperatures. An Apollo ND50 Single Flash Laser was used for determining room temperature values. This device was capable of measuring samples up to 3 millimeters thick. The second instrument was a Laser Applications 9300 Pulse Laser System. This system was used for the elevated temperature tests, but could only handle samples up to 2 millimeters thick. This limitation meant that the glass/vinyl ester laminates were thick to test at elevated temperatures, but tested at room temperature. A small thin disc of about 6 millimeters radius was subjected to a radiant energy source, a laser. The thermal diffusivity was calculated from the time required for the back face of the specimen to reach a certain percentage of its maximum value. This test is only performed at selected temperatures. The test was conducted at 126, 205, 272, and 342°C to build an adequate representation of the change in thermal diffusivity as a function of temperature.

2.5 Off Axis Stiffness Reduction

2.5.1 Test Motivation

The stiffness of polymers and polymer composites decreases at elevated temperatures. Off axis or matrix dominated lamina properties like shear and transverse moduli are most affected by matrix stiffness changes. This loss in stiffness must be characterized accurately if a predictive mechanical model is to be developed for elevated temperatures. Dynamic mechanical analysis (DMA) was implemented to determine the extent of stiffness loss over specified temperature ranges. DMA is a widely used small scale test used to determine modulus loss and the glass transition temperatures (T_g).

2.5.2 Test Description

The samples were tested using a TA Instrument DMA 2980 in a 3 – point bend deformation mode. Samples were tested at an orientation of 90° to capture the transverse stiffness loss as accurately as possible. Tests consisted of applying a sinusoidal load to the sample at a constant frequency 1 Hz. The sample temperature was increased from room temperature to 200°C at a constant rate of $5^\circ\text{C}/\text{min}$. Nominal sample dimensions were 55 mm in length and 15 mm wide.

2.6 Combined Thermal & Compressive Loading

2.6.1 Test Motivation

The motive for conducting this test was to characterize the response of a composite exposed to a “worst case” scenario. The test combined elevated temperatures with mechanical loading. The mechanical was a constant compressive load. Compression was chosen because the matrix material, which was high susceptible to elevated temperatures, dominated the compressive and buckling failures. Also many applications of composites are subject to compressive loading situations. Thus investigations into the mechanisms of their response and collapse under combined loading was important.

2.6.2 Test Description

The test was performed using multiple load applicators (thermal and mechanical), and was instrumented to record various test parameters over the duration of the test. The samples were machined to approximately 100 mm long by 25 mm wide. Samples were subjected to compressive stress levels from 14 to 40 MPa, while also being exposed to a steady heat flux of 5 to 30 kW/m². The samples were gripped longitudinally in a servo – hydraulic testing frame, exposing a 50 mm gage length. A constant compressive load was then applied to the sample. After the compressive load had ramped up to its final constant value an, infrared (IR) strip heater (Research Inc.) applied a constant heat flux to one side of the sample Figure 2-1. The IR heater uses a quartz lamp and a parabolic reflector to produce an approximately uniform heat flux over the gage length of the samples. The samples were painted black with a high temperature manifold paint to assure an absorptivity of approximately 0.95. Multiple gages and probes were used to monitor and control the test. Front (side exposed to the heat flux) and back side temperatures were recorded using small gage K-type thermocouples that were adhered to the surface using a dot of a standard epoxy. The applied heat flux was monitored and recorded using a Vatell HFM7-E/H heat flux gage, which has a maximum face temperature of 700 °C and a response time of 6 μsec. The heat flux gage was mounted flush to the lamp side surface of the composite samples that were tested. To achieve a constant applied heat flux, the gage was monitored real time during each run. If the heat flux drifted the power to the lamp was adjusted accordingly to keep the heat flux as stable as possible. The strains on the back side of the sample were measured with a Fiedler Optoelektronik GmbH laser extensometer over a gage length of approximately 45 mm. The laser extensometer used two reflective strips placed on the sample as references for the strain measurement. The laser extensometer cannot detect out of plane strain. This will be discussed in further detail in the modeling section. A standard 89 KN load cell was used to monitor the applied mechanical loads. All data channels were wired into a National Instruments Multiplexor Data Acquisition System, which allowed for real time monitoring of the variables and storage of the data.

2.7 Figures

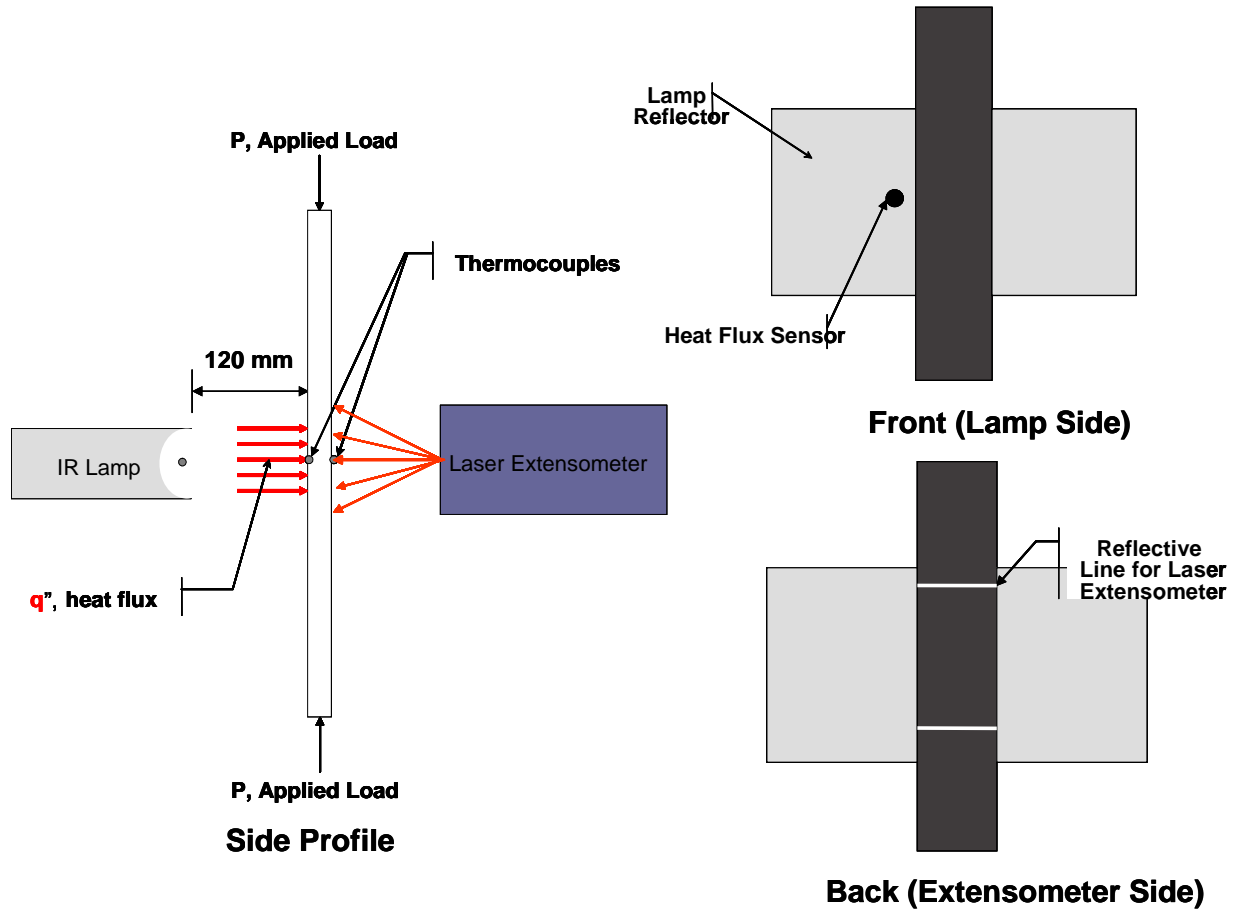


Figure 2-1: Combined Thermal Mechanical Loading Setup



Figure 2-2: Experimental Setup

CHAPTER 3 Experimental Results

3.1 Specific Heat

3.1.1 Acquired Data

DSC scans were performed on glass/vinyl ester and carbon/phenolic epoxy composites to determine the specific heat of the material as a function of temperature, from room temperature up to 300°C. The results for the glass/vinyl ester and carbon/phenolic epoxy are presented in Figure 3-1 and Figure 3-2 respectively.

3.1.2 Observations and Remarks

An increase in specific heat at approximately 250°C was observed for each material. This was thought to be due to the onset of thermal degradation as the thermal degradation process is endothermic. Thus, if the samples begin to degrade the amount of heat applied per second must increase to maintain the constant temperature rate increase.

The glass/vinyl ester experiment was started at room temperature and ramped up to 300°C, while the carbon/phenolic epoxy sample from at a sub ambient temperature and ramped to 300°C. For approximately the first 20°C of each experiment conducted, large fluctuations were observed. The fluctuations were unexplainable via any know material mechanism and were finally attributed to instrument noise during start up.

Even with the rapid increase at the higher temperatures the values do not vary drastically from the room temperature value. This suggested that the specific heat of these materials is essentially constant from room temperature until the onset of degradation. The T_g transition for each material system was not clearly observable from these experiments.

3.2 Thermal Diffusivity

3.2.1 Acquired Data

Thermal diffusivity at elevated temperature was collected only for the carbon/phenolic epoxy material because of the limited sample thickness that could be used with the instrument. Thermal diffusivity of the carbon/phenolic epoxy samples were collected over a temperature

range from room temperature to 350°C. The data is presented in Table 3-1 and plotted in Figure 3-3.

Table 3-1: Carbon/Phenolic-Epoxy Thermal Diffusivity

Temperature (°C)	21	126	205	272	342
Thermal Diffusivity (m ² /sec)	4.5018 E-07	3.1424 E-07	2.6762 E-07	2.4273 E-07	2.1392 E-07

The room temperature (21°C) thermal diffusivity that was determined for the vinyl ester/glass material was 2.5500 E-07 [m²/sec].

3.2.2 Observations and Remarks

Because the thermal diffusivity at elevated temperatures was not attainable for the glass vinyl ester composite, an assumption was made that the trend or shape of the thermal diffusivity curve for the glass/vinyl ester composite was the same shape as the carbon/phenolic epoxy curve, only with a varying initial room temperature value. This assumption was based on reviewing other materials and their thermal diffusivities. The phenolic-epoxy/carbon diffusivity data was normalized to the 21°C value. That is, all data points reported in Table 2-1 were divided by 4.5018 E-7 [m²/sec], the room temperature value for the carbon/phenolic epoxy sample. The resulting numbers are plotted in Figure 3-4, and an equation was fit to the data that is presented on the graph and in Equation (3-1).

$$y[T] = -0.1841 \ln[T] + 1.5687 \quad (3-1)$$

To construct the G/VE thermal diffusivity curve the right hand side of Equation (3-1) is simply multiplied by the room temperature G/VE diffusivity, the result is Equation (3-2) and is plotted in Figure 3-5.

$$y[T] = -0.466E-8 \cdot LN[T] + 3.98E-7 \quad (3-2)$$

3.3 Off Axis Stiffness Reduction

3.3.1 Acquired Data

The results of the DMA experiments are presented in Figure 3-6. Both curves were normalized, or divided by the room temperature values. It was assumed that the E₂₂ stiffness reduction on a ply level behaved similarly, (exhibited the same shape as the normalized stiffness

loss curves reported for each material). For the purpose of determining the ply level off axis stiffness reductions the normalized curves were scaled, (multiplied by the room temperature E_{22} values reported in Table 2-1 and Table 2-2). The scaled data is plotted in Figure 3-7

3.3.2 Observations and Remarks

The onset of stiffness reduction for the glass/vinyl ester sample was at a lower temperature than that of the carbon/phenolic epoxy sample. The final reduction levels at 200°C show the carbon/phenolic epoxy sample had essentially zero transverse stiffness while the glass/vinyl ester sample seemed to bottom out at 6% of the room temperature stiffness. This residual stiffness was thought to be a result of the fibers in the off axis directions continuing to contribute stiffness.

3.4 Combined Thermal & Compressive Loading

3.4.1 Acquired Data

The combined thermal and mechanical loading experiments were conducted only on the glass/vinyl ester material. The applied heat fluxes were 5, 6, 7, 8, 10, 15, 20 and 30 [kW/m²]. Extensive replicates were conducted at 5, 10, 15 and 20 [kW/m²]. At these heat flux levels applied compressive stresses were in the range of 10 to 40 [MPa]. For each experiment the strain on the unexposed side, front and back temperatures, applied heat flux, and times to failure were recorded.

An example of the recorded data is provided in Figure 3-8. This figure shows the recorded strain along with the front and back face temperatures. The strain profile reads zero until about 5 seconds when the compressive load is applied. The linear increase in compressive strain corresponds to the mechanical loading. The strain then plateaus for a few seconds. This provides a paused intended as a break point to allow for application of the heat flux at a distinctly different time from the mechanical load. At 20 seconds the front temperature begins to rise. This signifies application of the external heat (the IR lamp was turned on at that moment). A few seconds later the back temperature begins to rise; this delay results from the time required for the heat to diffuse through the thickness of the sample to the back face. It is noteworthy that the strain also begins to positively increase, (corresponding to an elongation) at the same moment as the application of the heat flux. The strain profile continues to increase until the 80

second mark, when the samples ceases longitudinal expansion and begins compressing. The strain falls steadily with time, causing failure to occur at 140 seconds, indicated by the catastrophic increase in compressive strain. Further explanation of the observed strain profiles is presented in the next section.

The front and back temperature profiles for each experiment at heat fluxes of 5, 10, 15, and 20 kW/m² are presented in Figure 3-9 through Figure 3-12. For each flux level, the average front and back temperature profiles were calculated and plotted on the graphs. The upper curve is the average front side (exposed side) temperature, and the lower red curve is the back side average temperature. Time zero for the plots corresponds to the moment of the activation of the heat lamp. The average front and back temperatures for each heat flux level were determined and plotted in Figure 3-13.

The strain profiles for each specimen tested at their respective heat flux levels are plotted in Figure 3-14 through Figure 3-17. Each plot is grouped by heat flux level, where time zero also corresponds to initiation of the thermal loading. The legend in each graph lists the applied compressive stress on each specimen. For some of the plots there are circle indicators noting the specimens that did not fail, (i.e. run out) but that were stopped after an extended time, either 1 hour or 30 minutes.

A phenomenon that was termed “maximum strain shift” is presented in Figure 3-18 through Figure 3-21. These plots are the same as the strain profile plots in Figure 3-14 through Figure 3-17, except that the plot region is focused around the maximum of the curves. Trend lines are fit to the plots to indicate the shift in time of the maximum strain.

The change in strain was calculated from the strain response and is plotted in Figure 3-22 through Figure 3-25. The area plotted is focusing in close to reveal the initial change in strain values for the specimens.

And finally, a failure surface was constructed for the times to failure of each sample versus applied compressive stress and heat flux. The resulting plot is depicted in Figure 3-27.

3.4.2 Observations and Remarks

3.4.2.1 Temperature Conditions

The temperature profiles reported at the variety of heat fluxes exhibited substantial variations from the averages. One source of the deviation, at least for the front side temperature measurement could be due to the fact the thermocouples were bonded to the surface using small dots of epoxy. This bonding process had inherent variability in it because of the hands on method employed. Each epoxy dot was not equal size, and the placement of the tip of the thermocouple inside the epoxy dot was inconsistent (i.e. height from the surface) due to the thermocouple moving during cure of the epoxy. The tip at times was close or touching the surface of the sample, and other times suspended in the epoxy dot. This small variation may contribute significantly to the variation in measured front side temperatures.

Because the front (exposed) side thermocouple was directly exposed to the heat flux from the lamp, the recorded temperatures might have been higher than the actual surface temperatures of the samples. This is due to the fact the thermocouple is directly absorbing heat from the lamp. This was in contrast to the back side thermocouples that were only reading temperatures from heat that had diffused through the samples. Moreover, both temperature measurements were influenced by convection. This influence added to the variability in the temperature measurements for each experiment.

Another source of temperature variation was due to variation in the applied heat flux between experiments and during the course of the test. The readings from the heat flux gage revealed that the applied heat flux sometimes drifted during the first minute of exposure. These drifts (1 or 2 kW/m²) could influence the induced temperatures. The drift was thought to be from the lamp warming up during use.

3.4.2.2 Strain Response

The initial positive strains in the strain profiles are attributed to the thermal expansion of the material. At temperatures lower than the T_g 's this thermal expansion was believed to be dominated by the off axis plies. The thermal expansion coefficient in the transverse direction was more than five times greater than in the longitudinal direction. The positive increase in strain continued until the temperature induced stiffness loss overcomes the thermal expansion.

The initial positive strain increase rate was directly proportional to the applied heat flux level, as would be expected. This positive rate of increase was independent of the applied compression load, as depicted in Figure 3-22 through Figure 3-25. The average strain rate was calculated for each heat flux level and is plotted in Figure 3-26.

Once the initial strain increase occurred, the strain reached a maximum and began to decrease. After this point the strains continued to decrease until final collapse of the specimen. At a given heat flux level this maximum shifted to longer or shorter times depending on the applied mechanical load. The solid black line in Figure 3-20 emphasizes the maximum strain shift phenomena. This shift occurred when the thermal strains were overcome by the applied mechanical load.

3.4.2.3 Creep Rupture under Compression

In an effort to organize and understand the creep rupture under compression results the times to failure for each sample were plotted versus compressive load. Results for each heat flux level were overlaid onto Figure 3-27. There are numerous trends in the figure worth noting. The arrow on the graph notes the trend in the observed times to failure with applied heat flux. As the heat flux is increased the times to failure decreased as expected. The higher the heat flux the more rapidly the sample reached temperatures near or above the T_g and failed. As the temperature approaches T_g the mechanical properties decrease due to the increase in the polymer chain mobility.

For all heat flux levels, there is a stress at which the times to failure switched failure modes. For example, the 10 [kW/m²] heat flux dataset; showed a nearly linear trend between applied compressive stress and failure times. This was true until the compressive stress was less than 13.8 [MPa]. At this stress, level a dramatic change in strain profiles occurred and the times to failure were greatly extended. This change in failure mode can be observed in the strain profiles for the 10 [kW/m²] heat flux level (Figure 3-15). At high loads the strain increased initially and then quickly decreased as the specimen approaches failure. At and above applied stress levels of approximately 13.8 [MPa] the decrease in strains was much more gradual. This was evidence for a second failure mechanism at lower loads. This threshold stress level was on the order of 14 [MPa] for all compressive load levels except the 5 [kW/m²] heat flux cases. In this case, the lower limit stress was approximately 30 [MPa].

The initial [0°] ply fiber undulation was investigated by taking a micrograph of a polished virgin sample. The initial fiber misalignment is minimal as seen in Figure 3-28. After the initial misalignment angle was determined the sample was tested at 5 [kW/m²] and a low mechanical load, approximately 27 [MPa]. This resulted in a run out, that is the sample did not collapse. The specimen was allowed to cool and another micrograph was taken. The picture gives proof of the existence of the kinking phenomena.

To further investigate the failure mode changes, each failed sample was sorted by failure mode, applied heat flux, and applied mechanical load. It was determined by visual inspection of failed samples there are four distinct failure modes Figure 3-29. Modes 1 and 2 are examples kink band formation. Mode 3 appears to be a crushing mode and Mode 4 was termed “double kink band”, because it appears to be a combination of Modes 1 and 2.

The overwhelming majority of specimens failed in Mode 1. Only a small few failed in the remaining modes and those specific mode failures occurred at or near the lower load threshold. As the mechanical loads decreased the mode switched from Mode 1 to one of the other modes. This is again evidence of a distinct switch in failure modes at the lower loads.

3.5 Figures

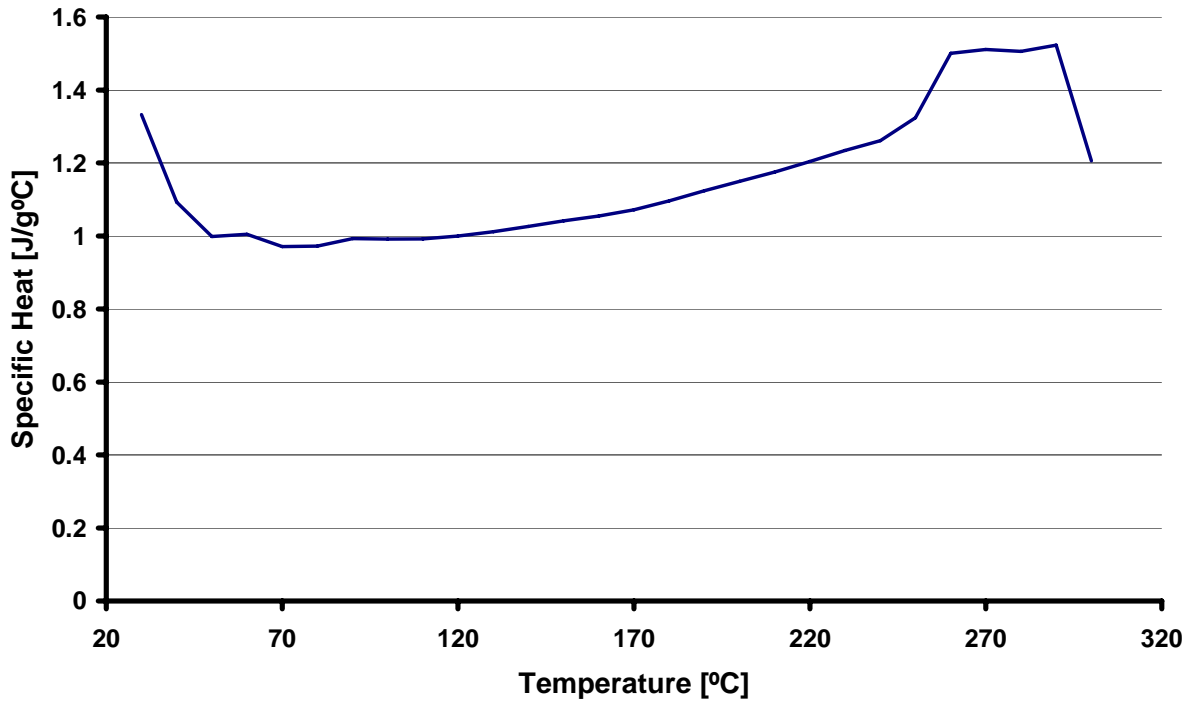


Figure 3-1: Specific Heat of Glass/Vinyl-Ester Composite

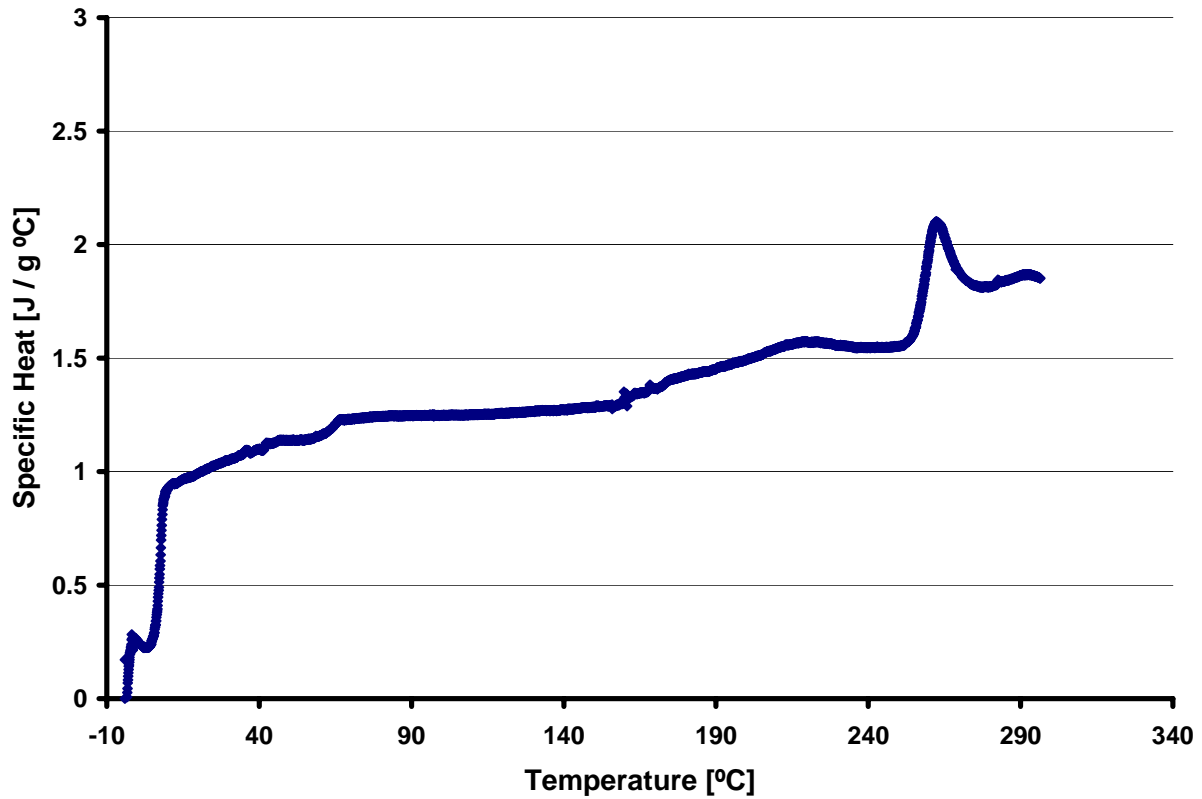


Figure 3-2: Specific Heat of Carbon/Phenolic-Epoxy Composite

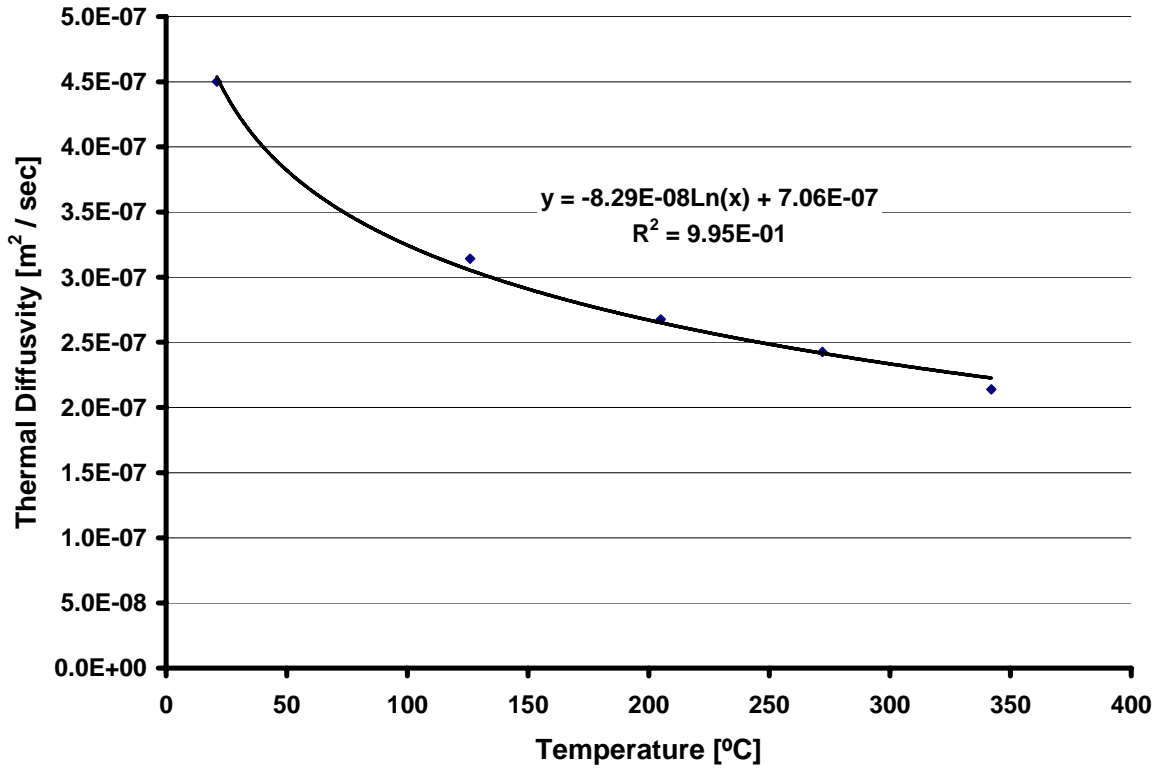


Figure 3-3: Thermal Diffusivity of Carbon/Phenolic-Epoxy Composite

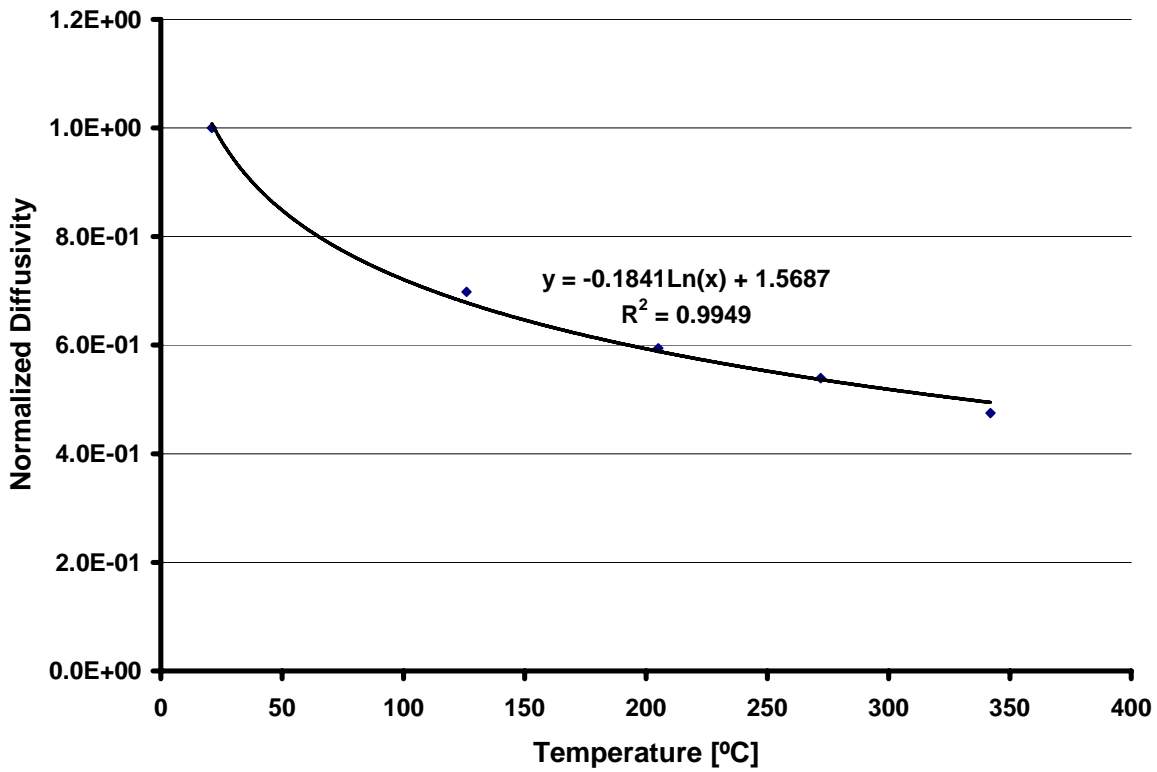


Figure 3-4: Thermal Diffusivity of Carbon/Phenolic-Epoxy Normalized to 21°C

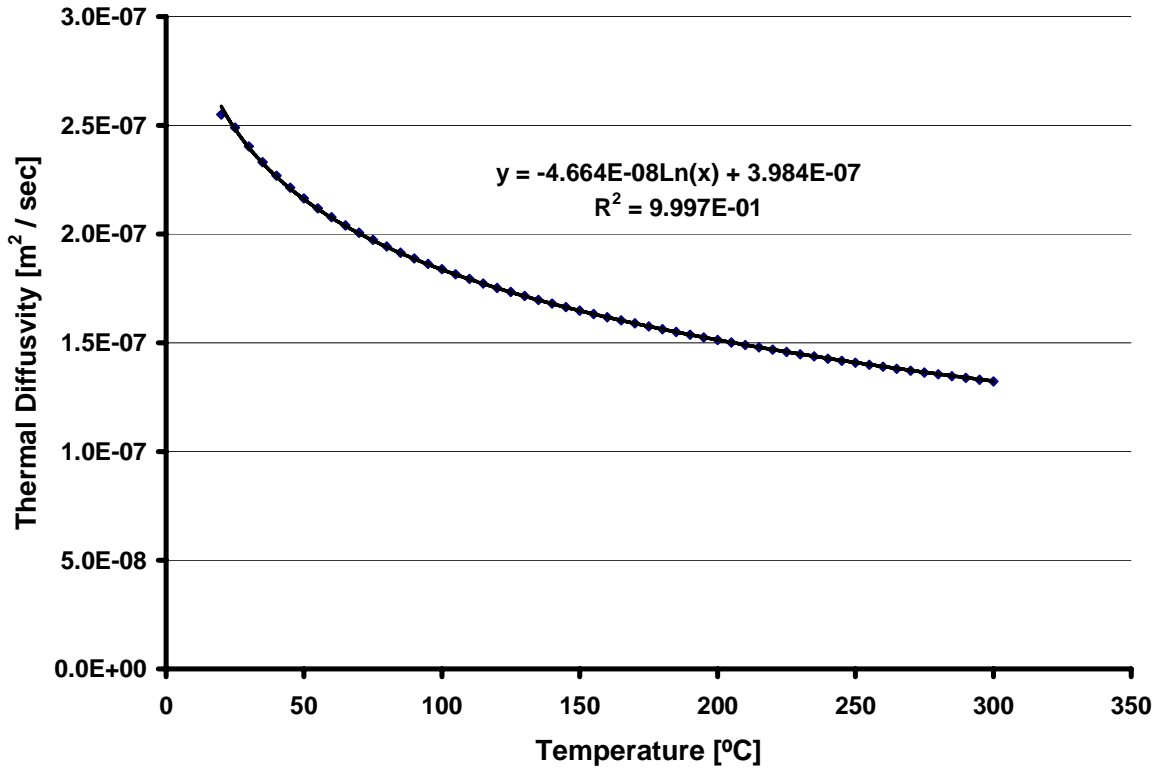


Figure 3-5: Thermal Diffusivity of Glass/Vinyl-Ester Composite

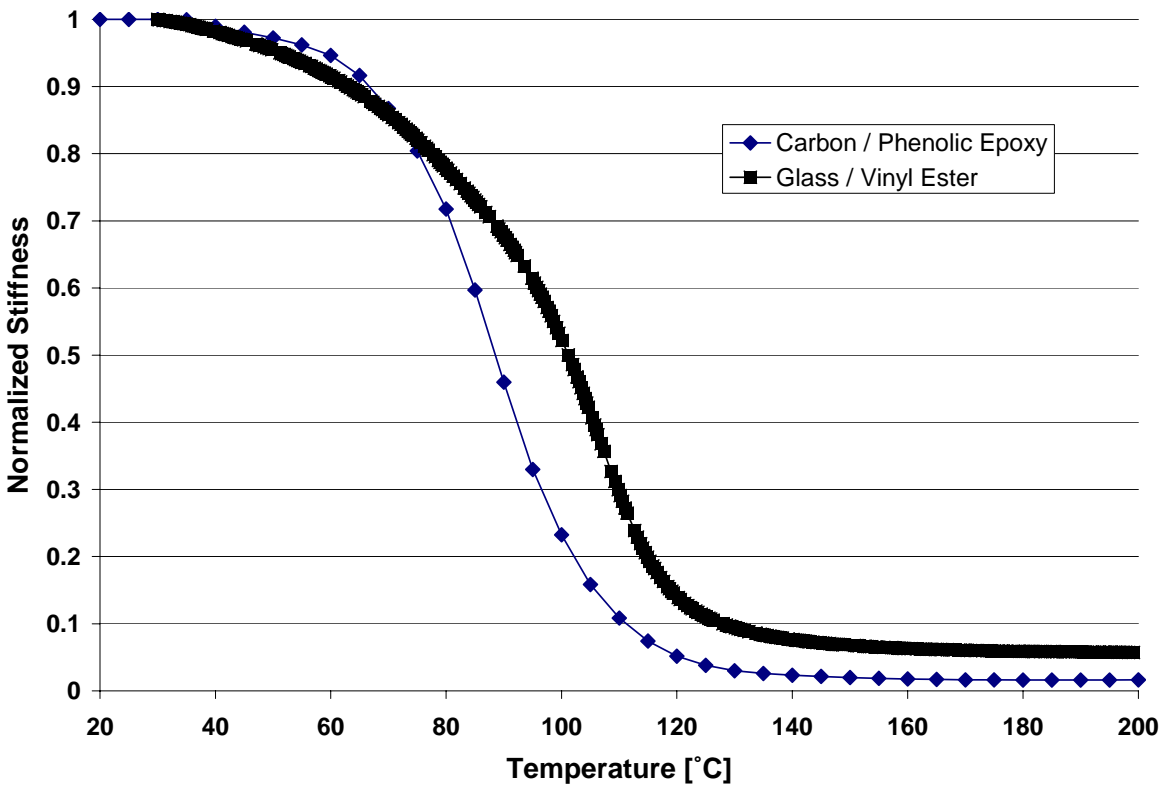


Figure 3-6: Stiffness Reduction Normalized to Room Temperature Value

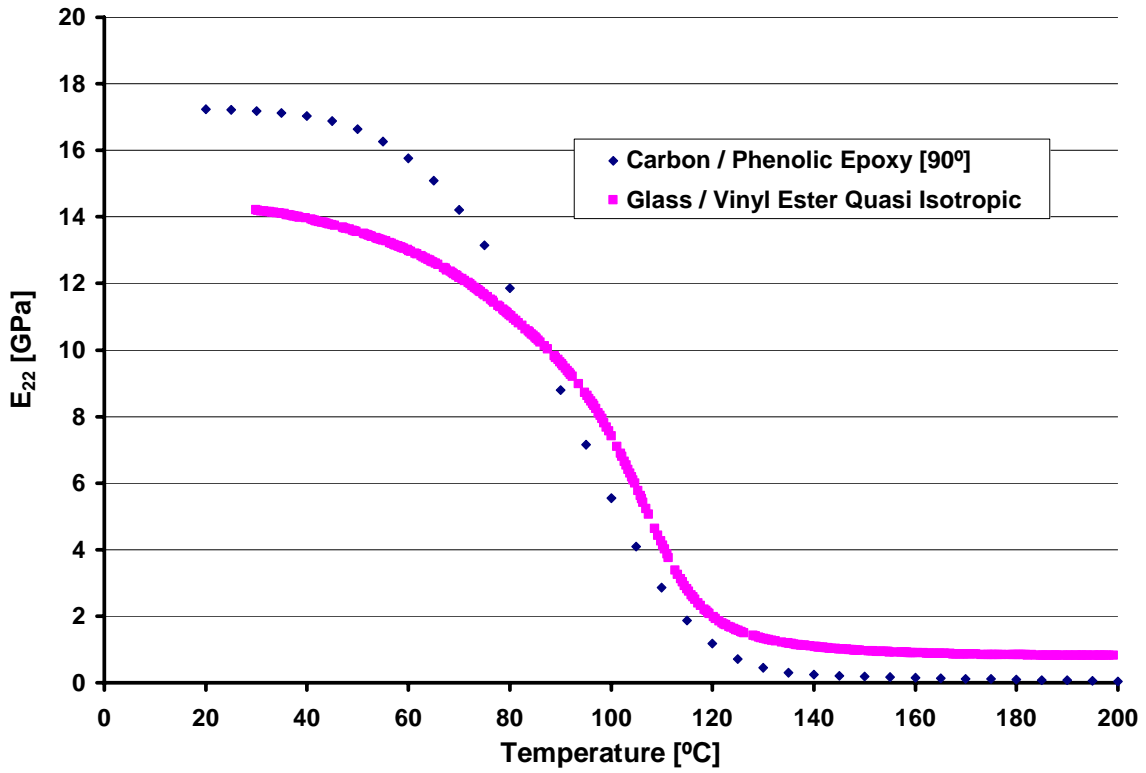


Figure 3-7: Scaled E_{22} Reduction Curves

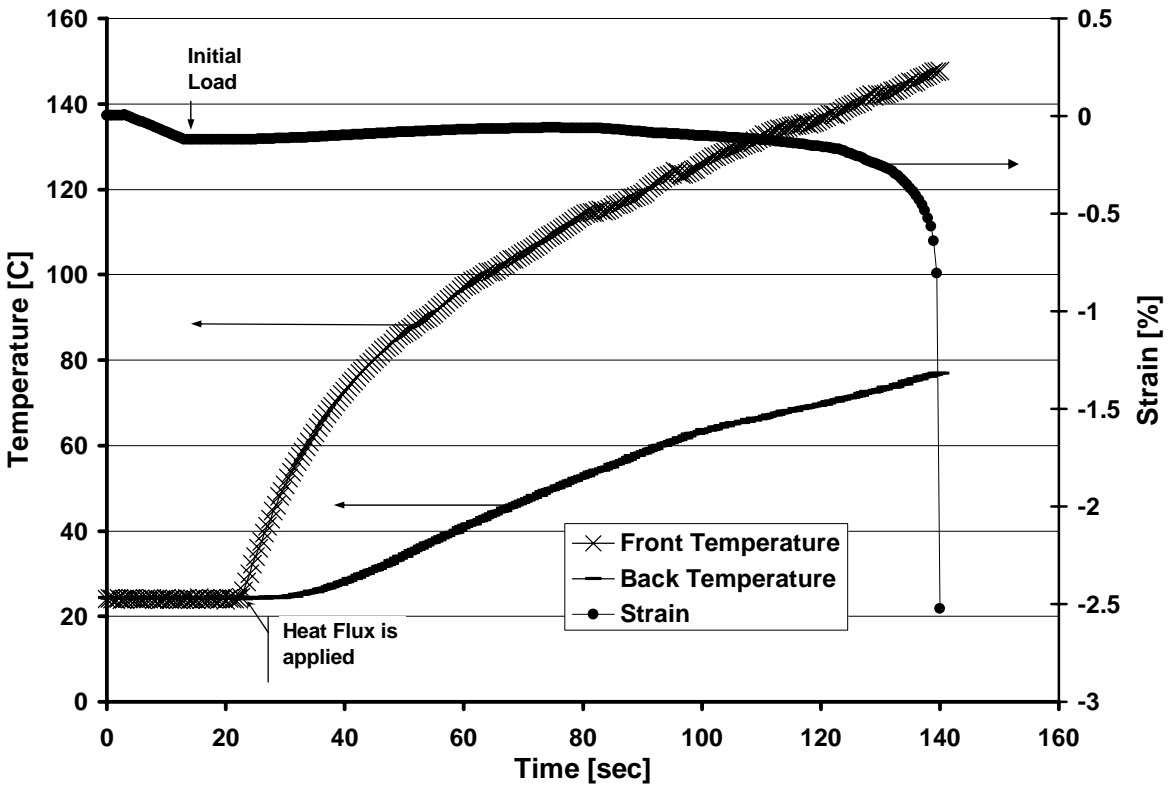


Figure 3-8: Example Test, Recorded % Strain, Front & Back Temperatures

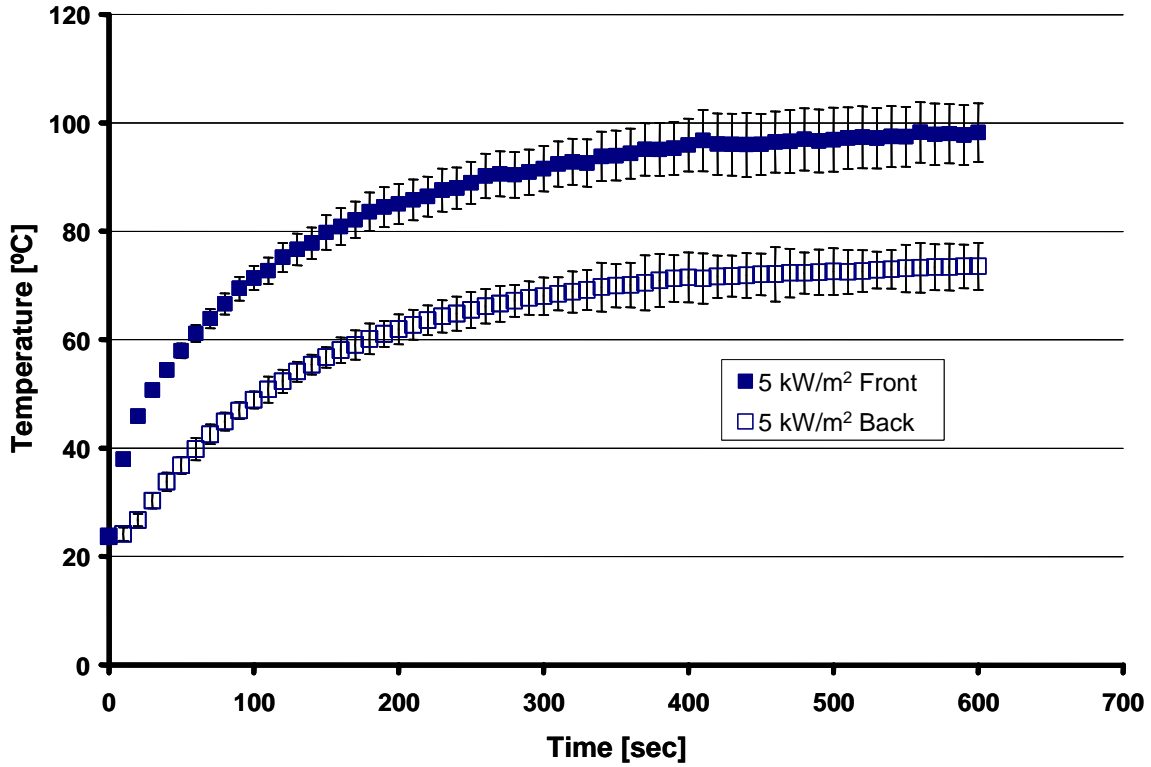


Figure 3-9: 5 [kW/m²] Temperature Profiles

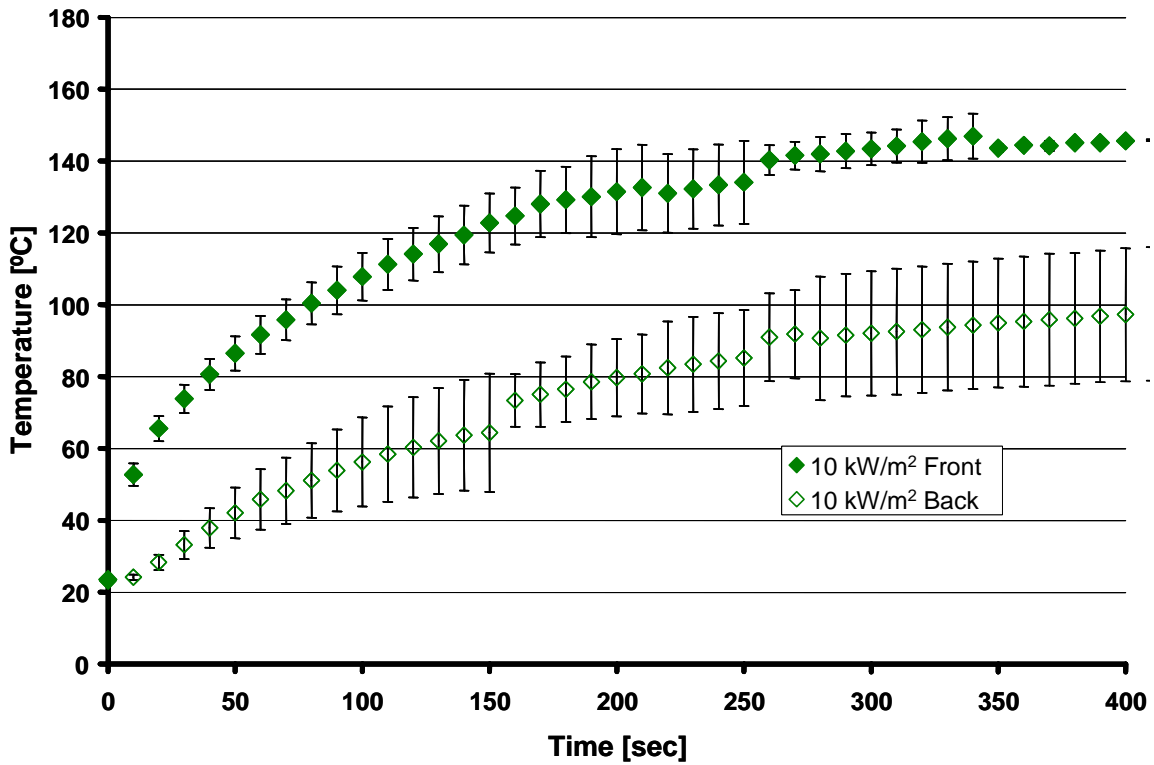


Figure 3-10: 10 [kW/m²] Temperature Profiles

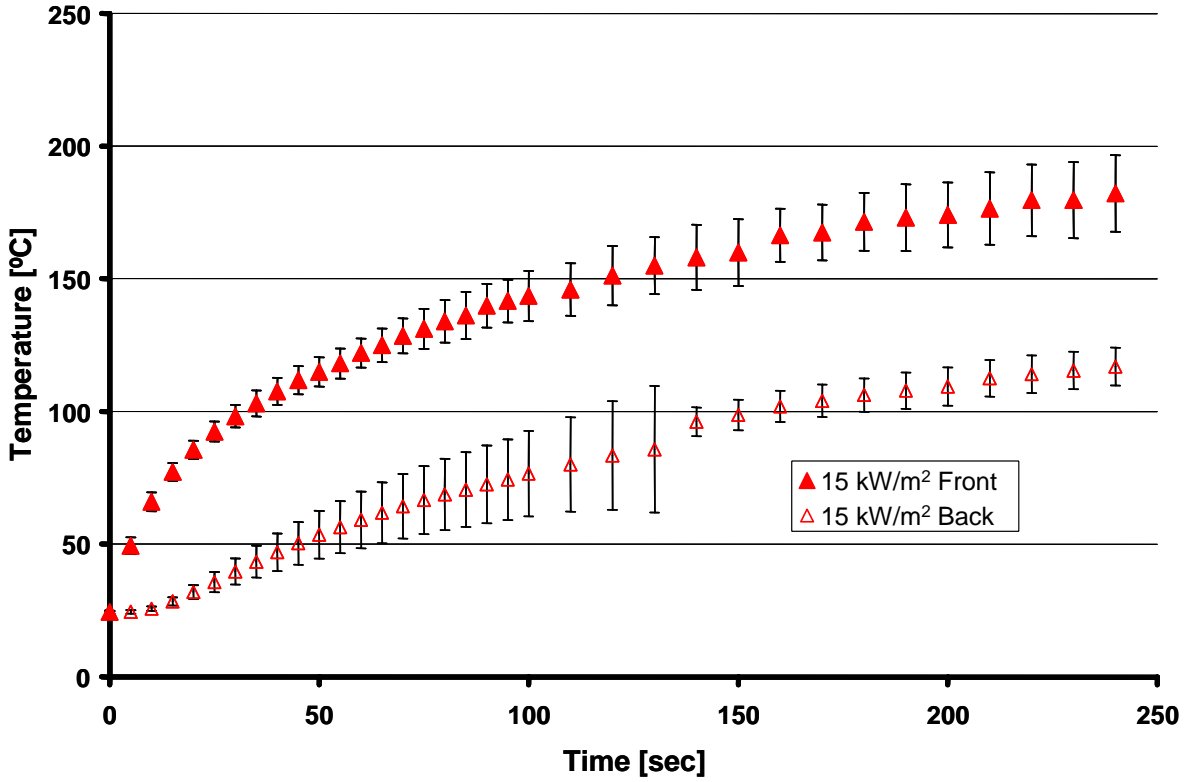


Figure 3-11: 15 [kW/m²] Temperature Profiles

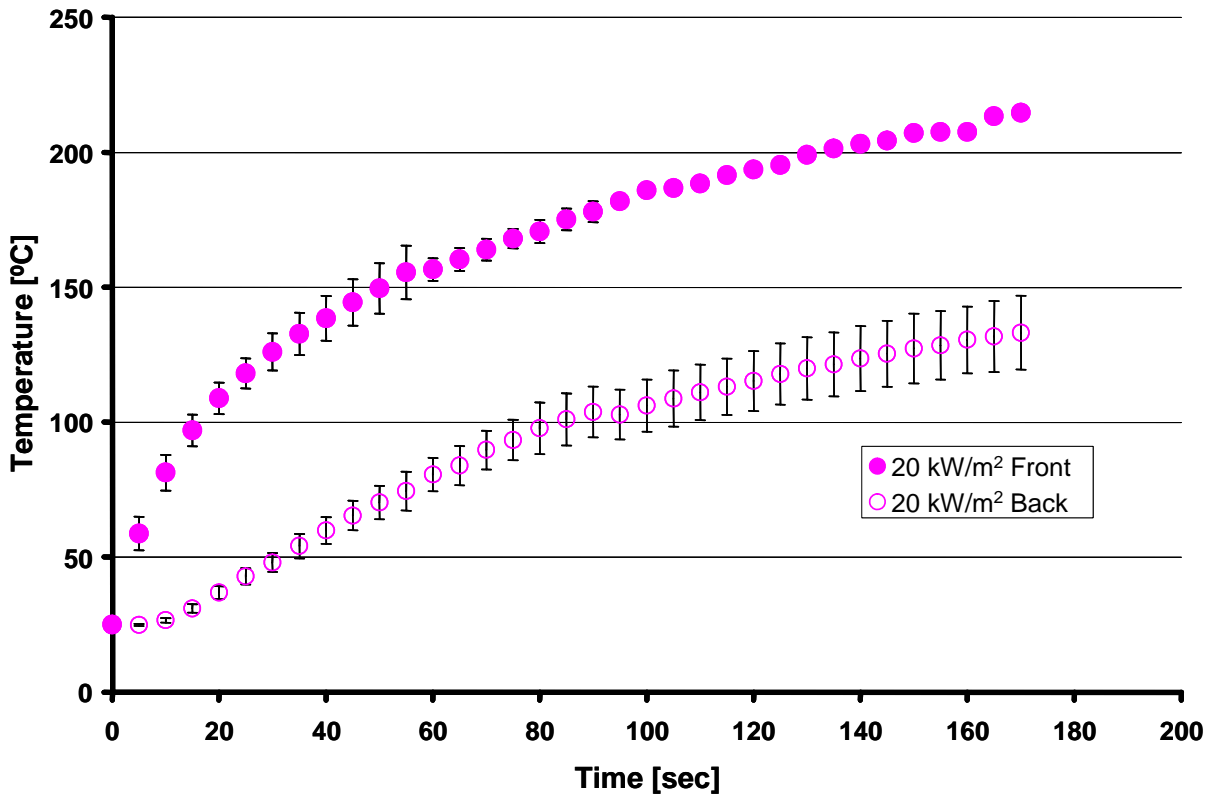


Figure 3-12: 20 [kW/m²] Temperature Profiles

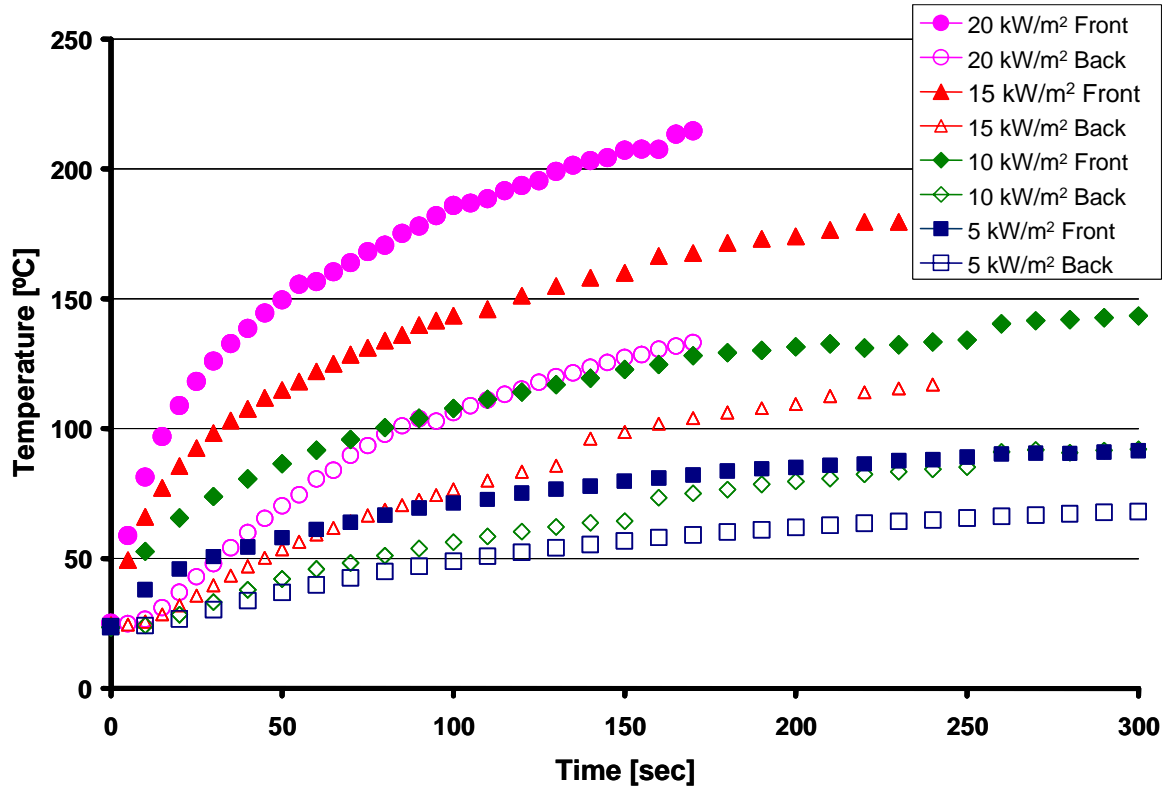


Figure 3-13: Average Temperature Comparison for All Heat Fluxes

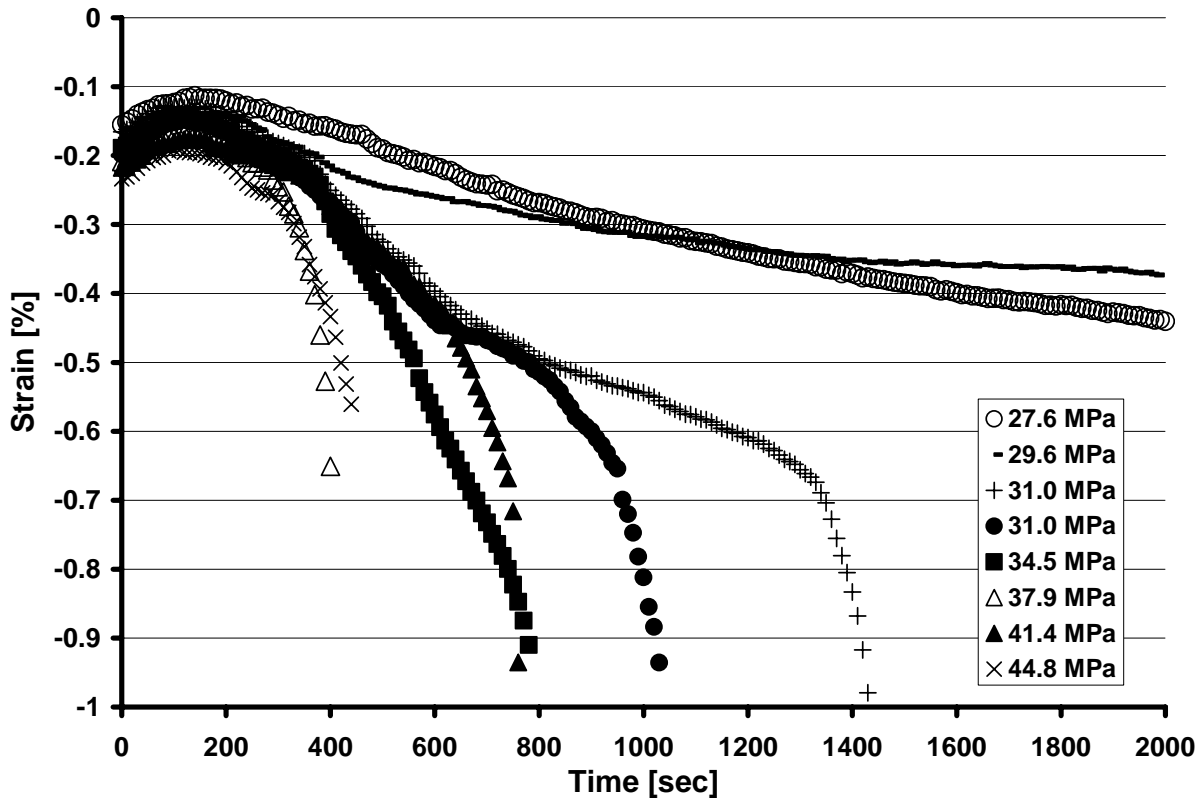


Figure 3-14: 5 [kW/m²] Strain Profiles

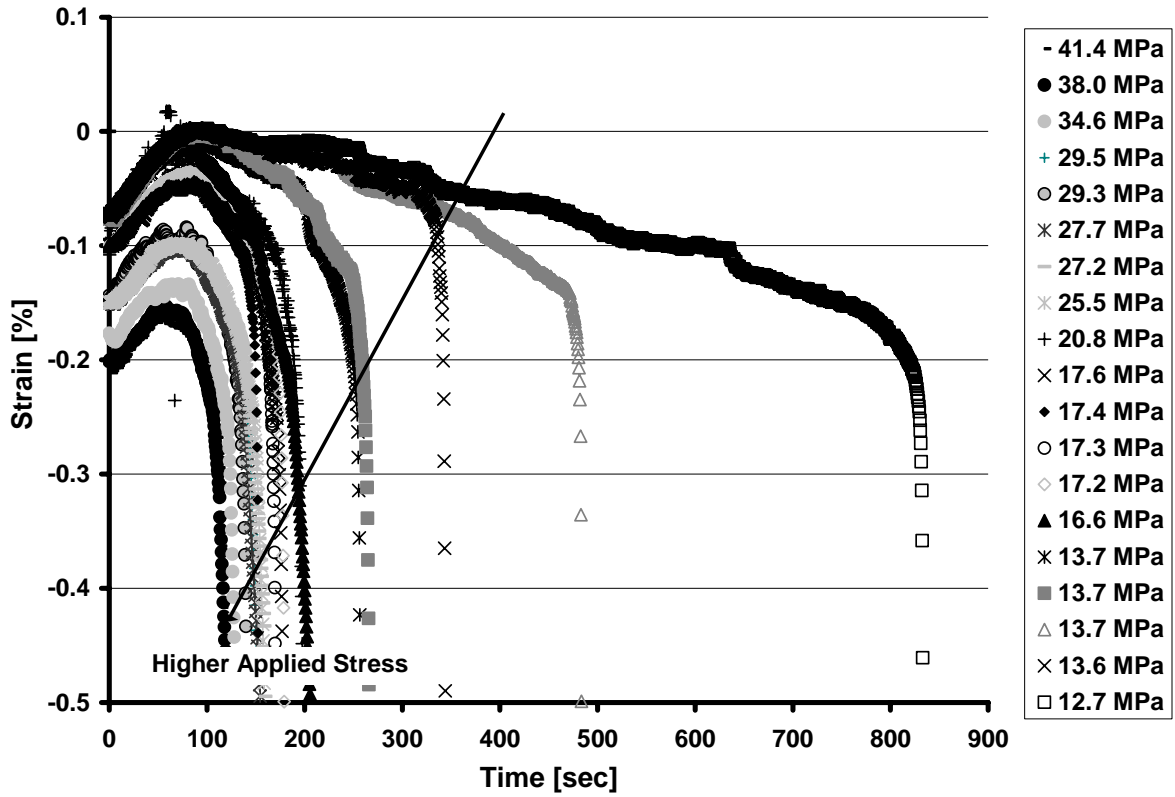


Figure 3-15: 10 [kW/m²] Strain Profiles

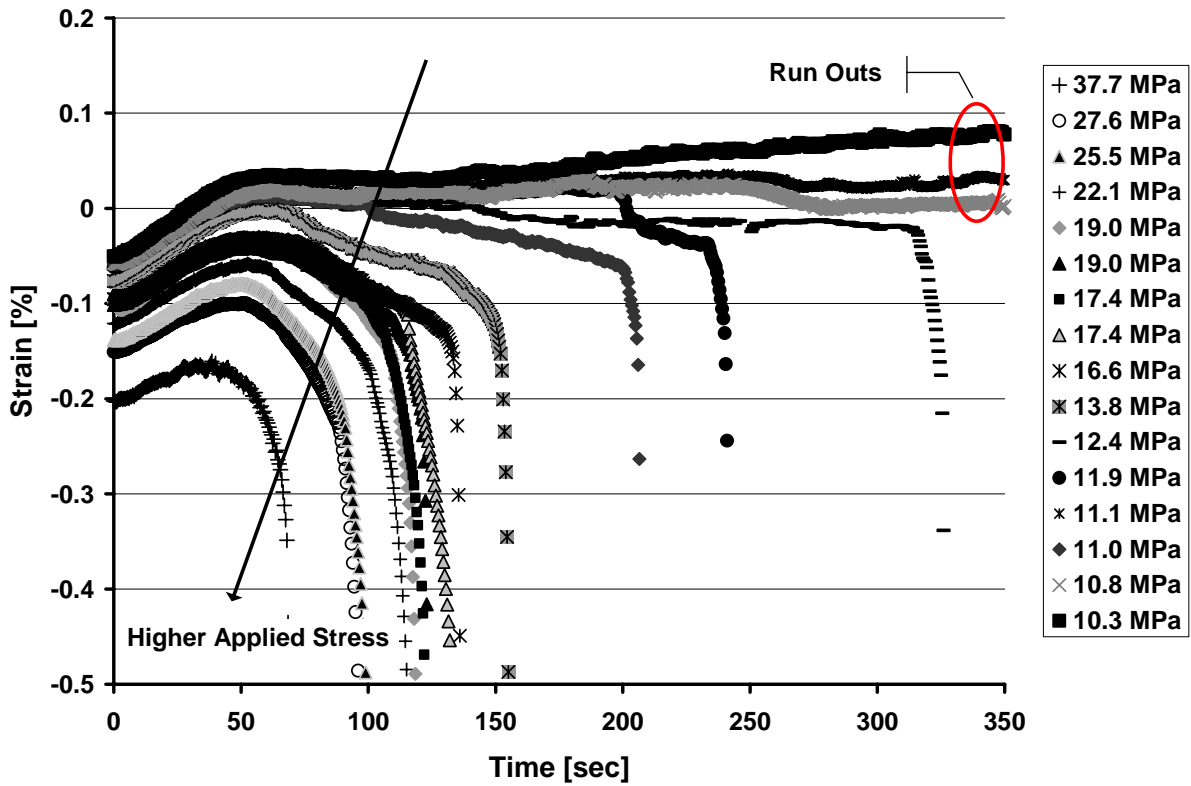


Figure 3-16: 15 [kW/m²] Strain Profiles

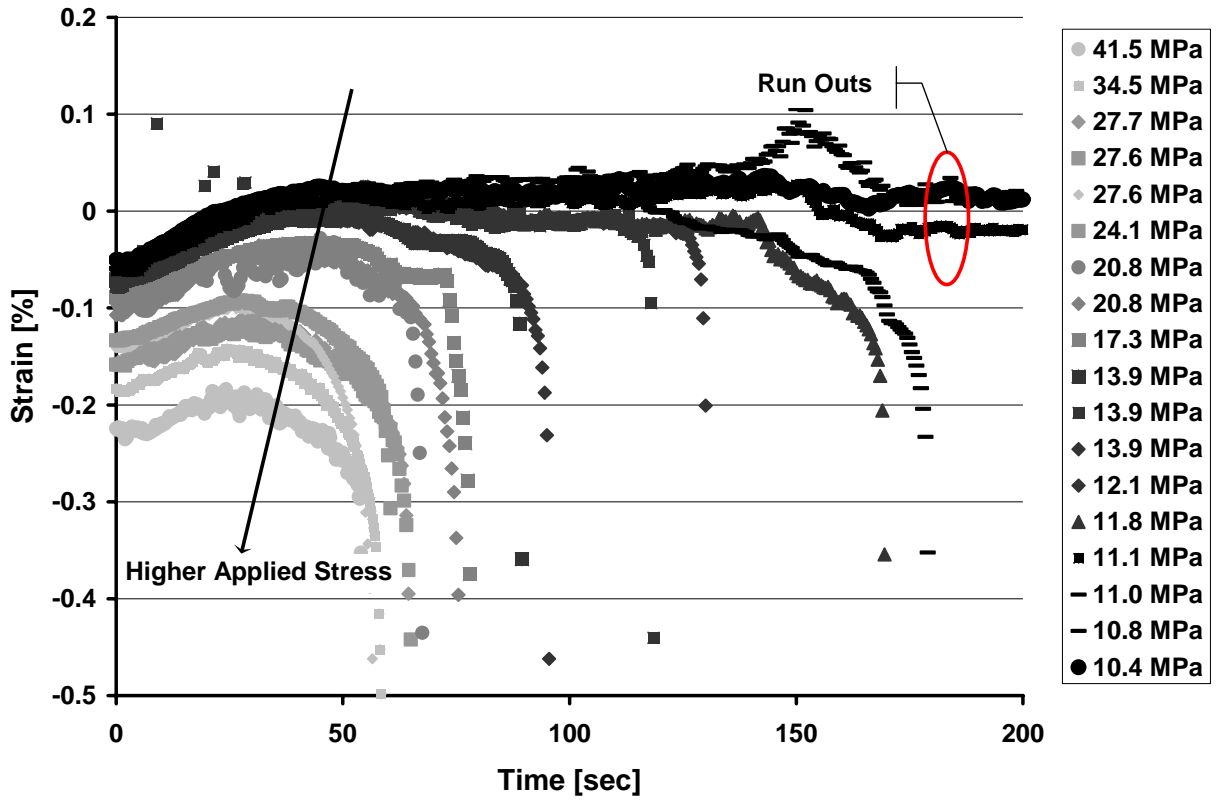


Figure 3-17: 20 [kW/m²] Strain Profiles

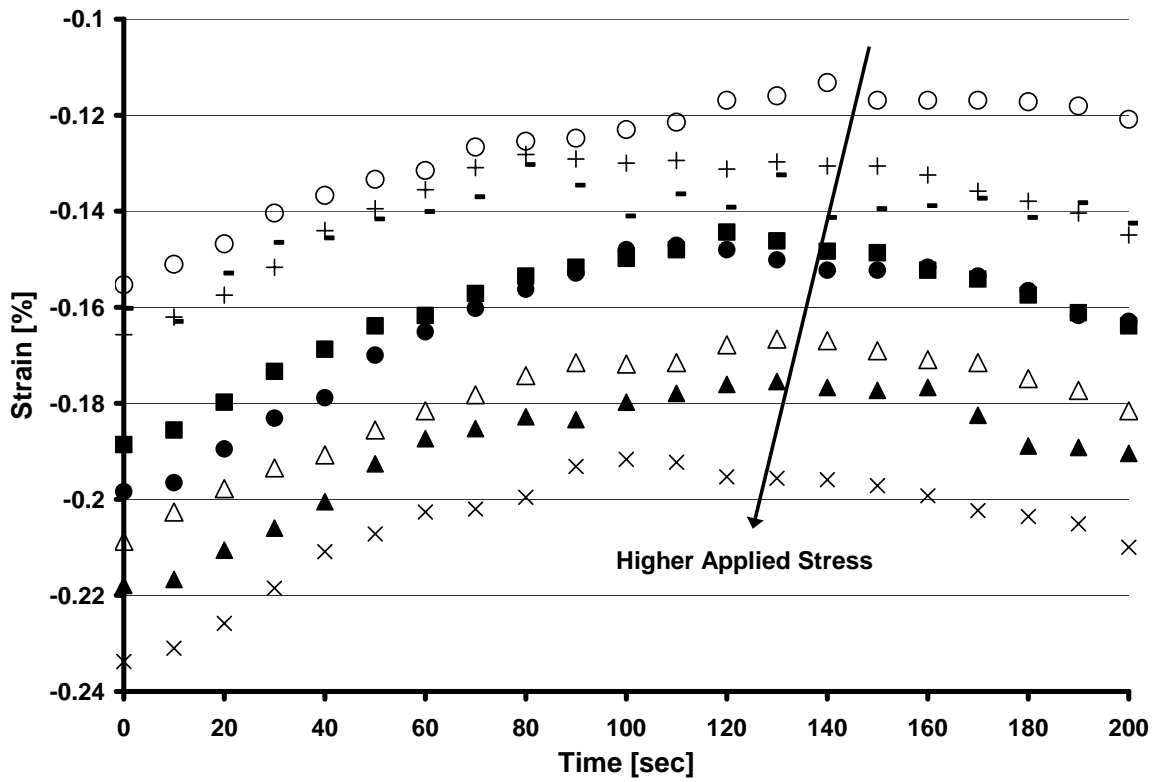


Figure 3-18: 5 [kW/m²] Maximum Strain Shifts

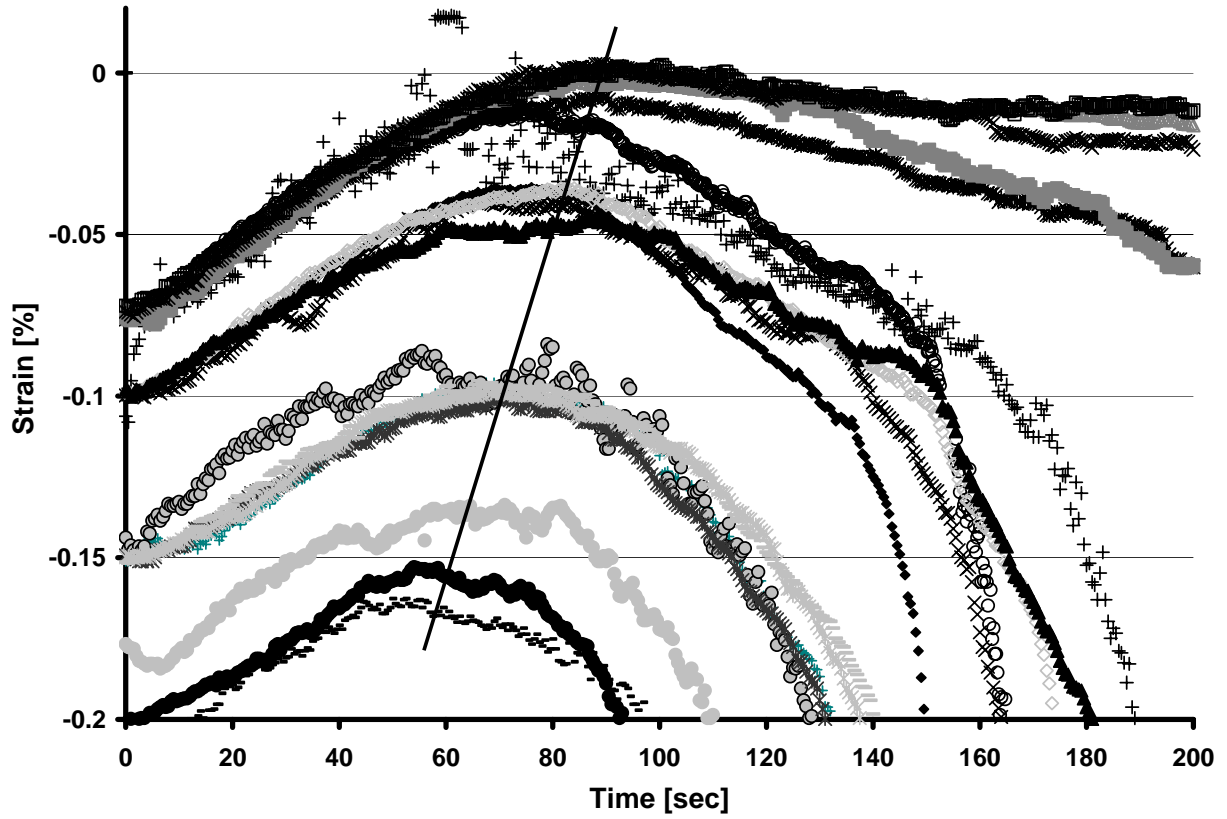


Figure 3-19: 10 [kW/m²] Maximum Strain Shifts

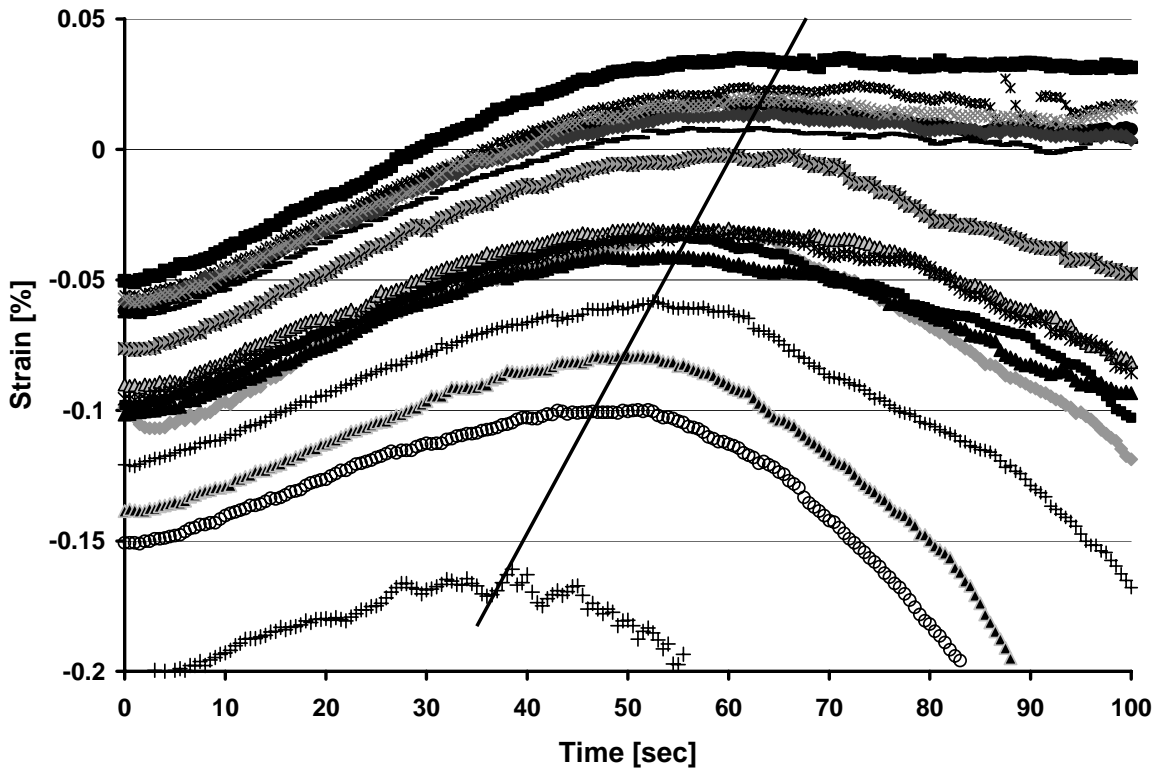


Figure 3-20: 15 [kW/m²] Maximum Strain Shifts

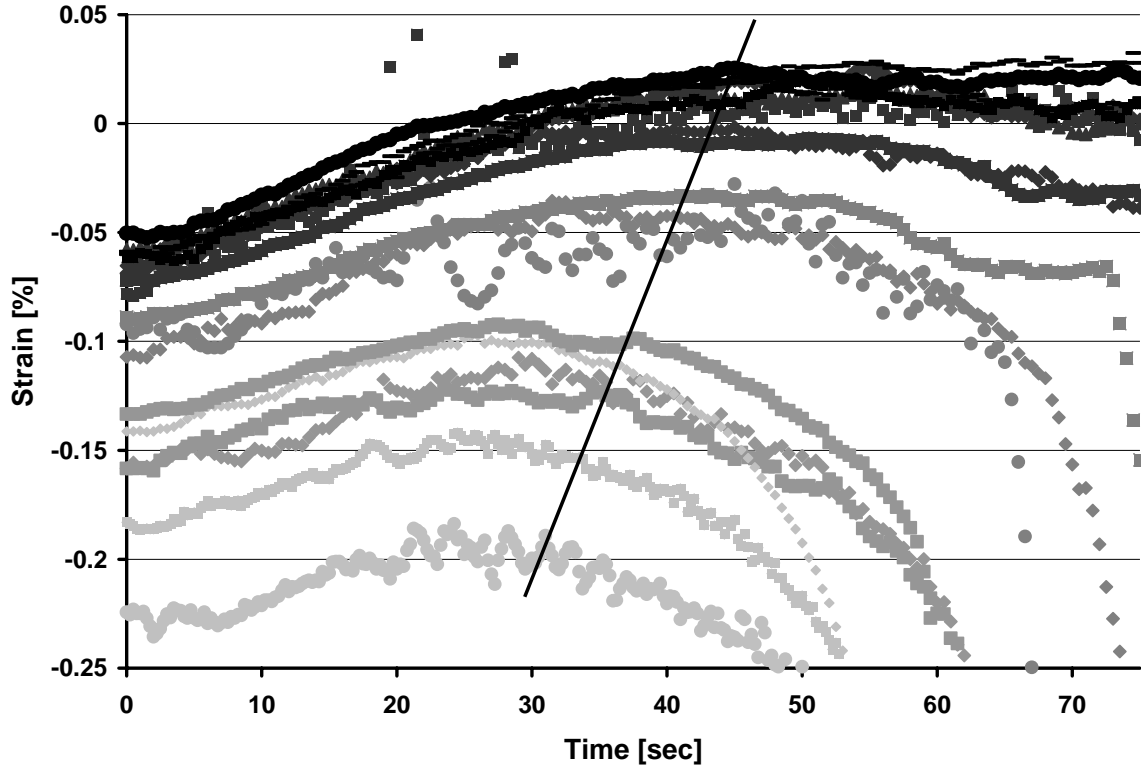


Figure 3-21: 20 [kW/m²] Maximum Strain Shifts

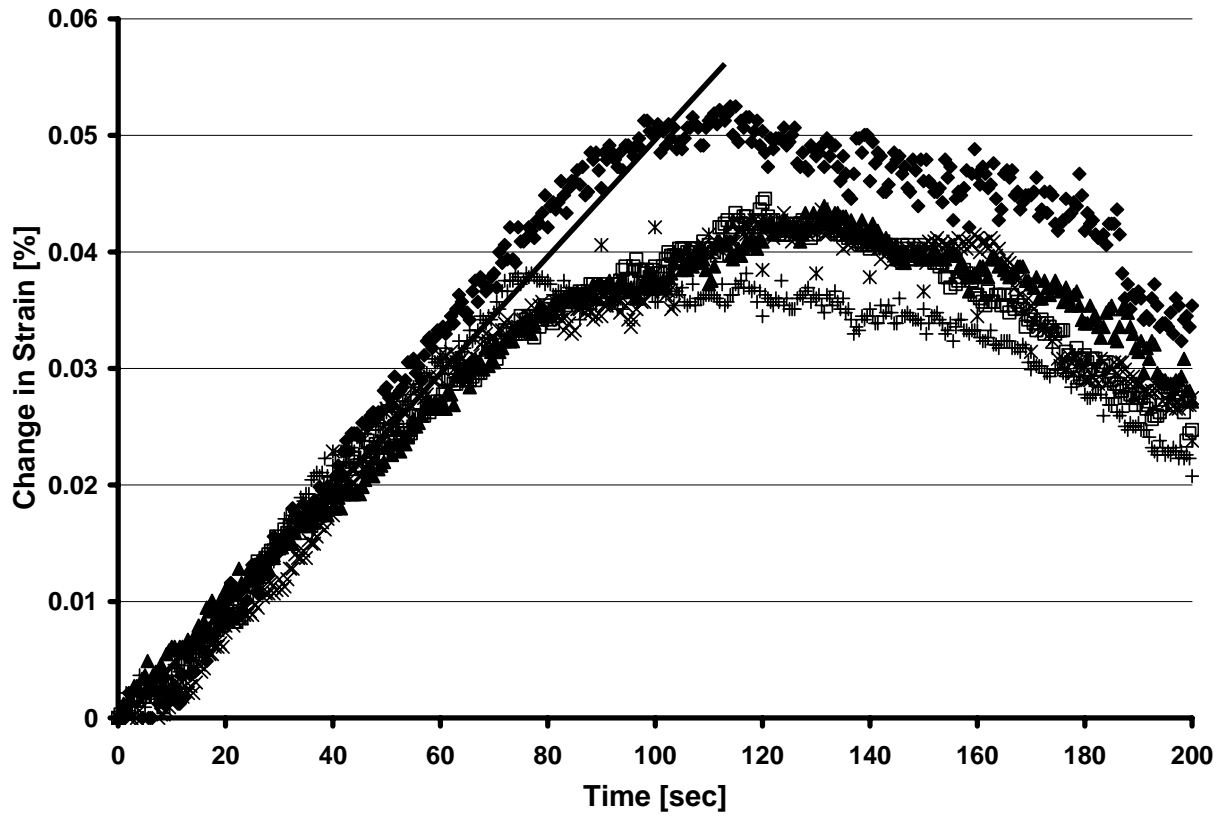


Figure 3-22: 5 [kW/m²] Change in % Strain Slope

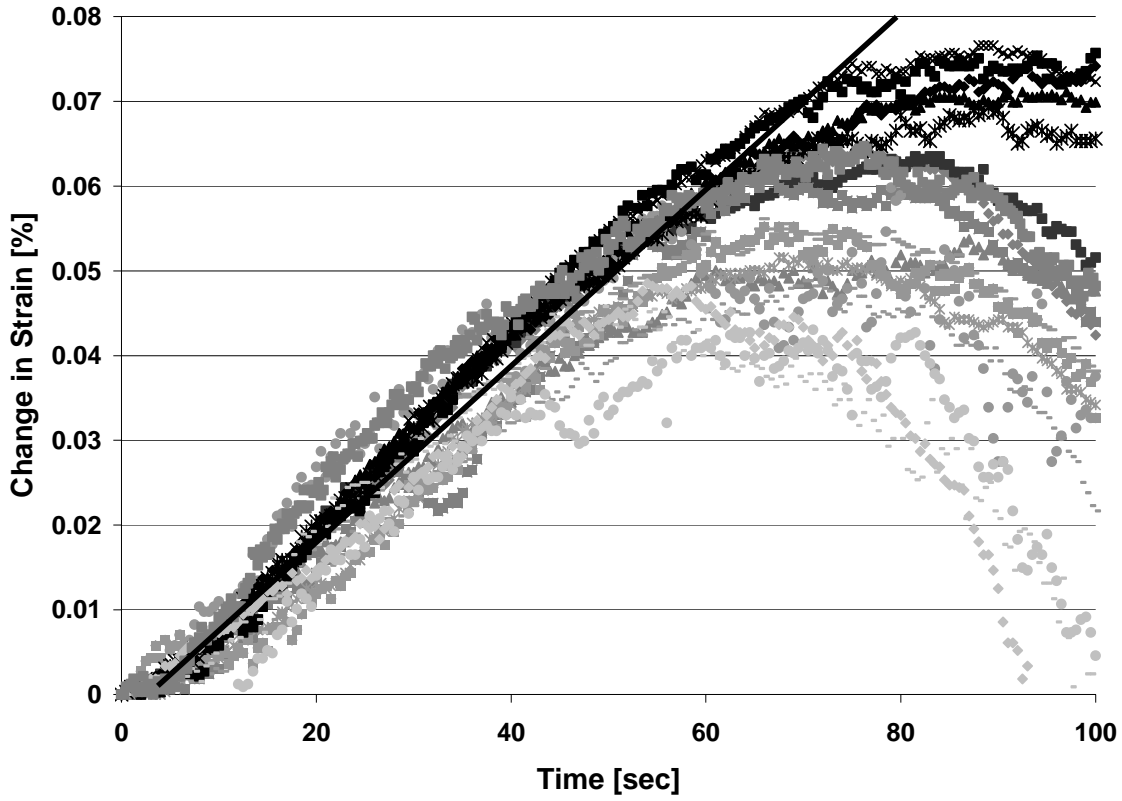


Figure 3-23: 10 [kW/m²] Change in % Strain Slope

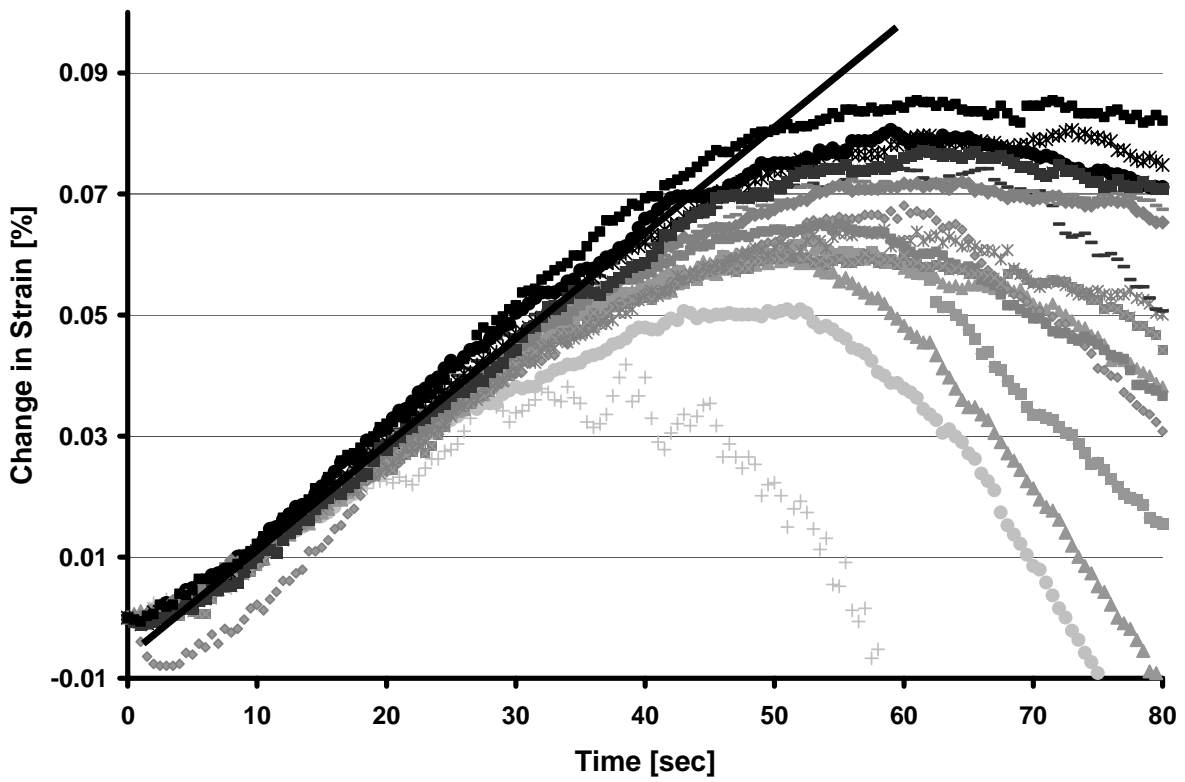


Figure 3-24: 15 [kW/m²] Change in % Strain Slope

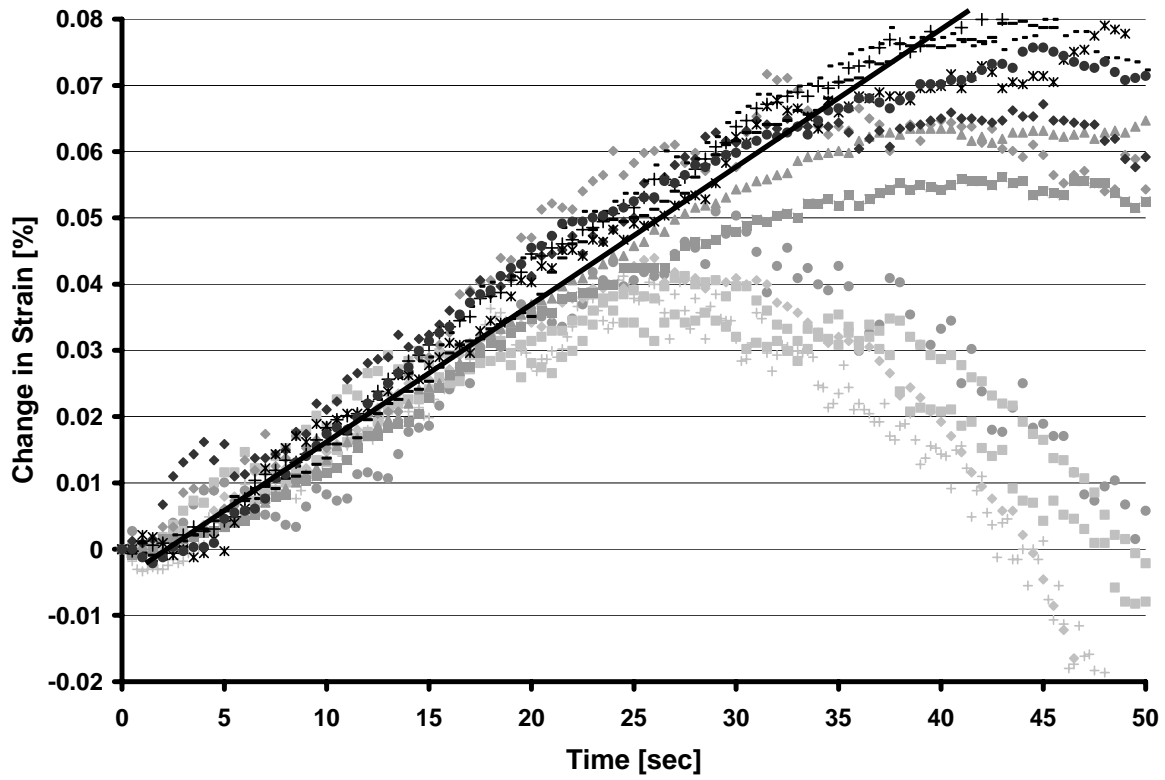


Figure 3-25: 20 [kW/m²] Change in % Strain Slope

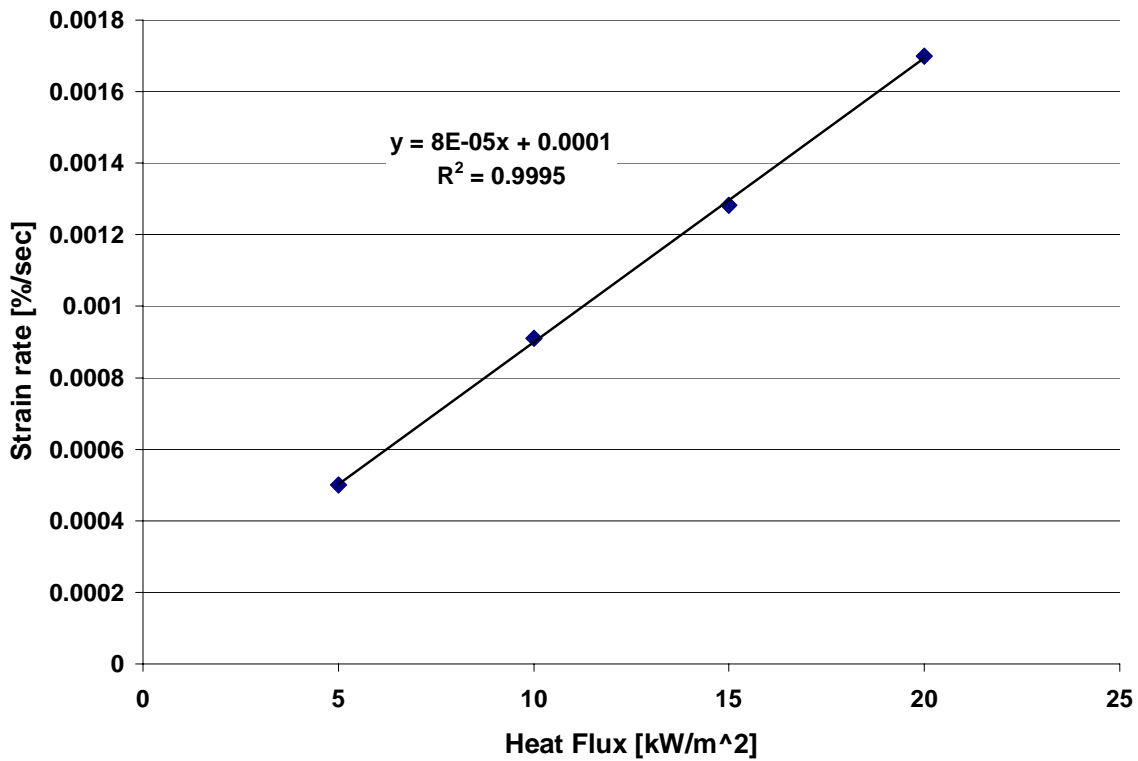


Figure 3-26: Initial Strain rate vs. Applied Heat flux

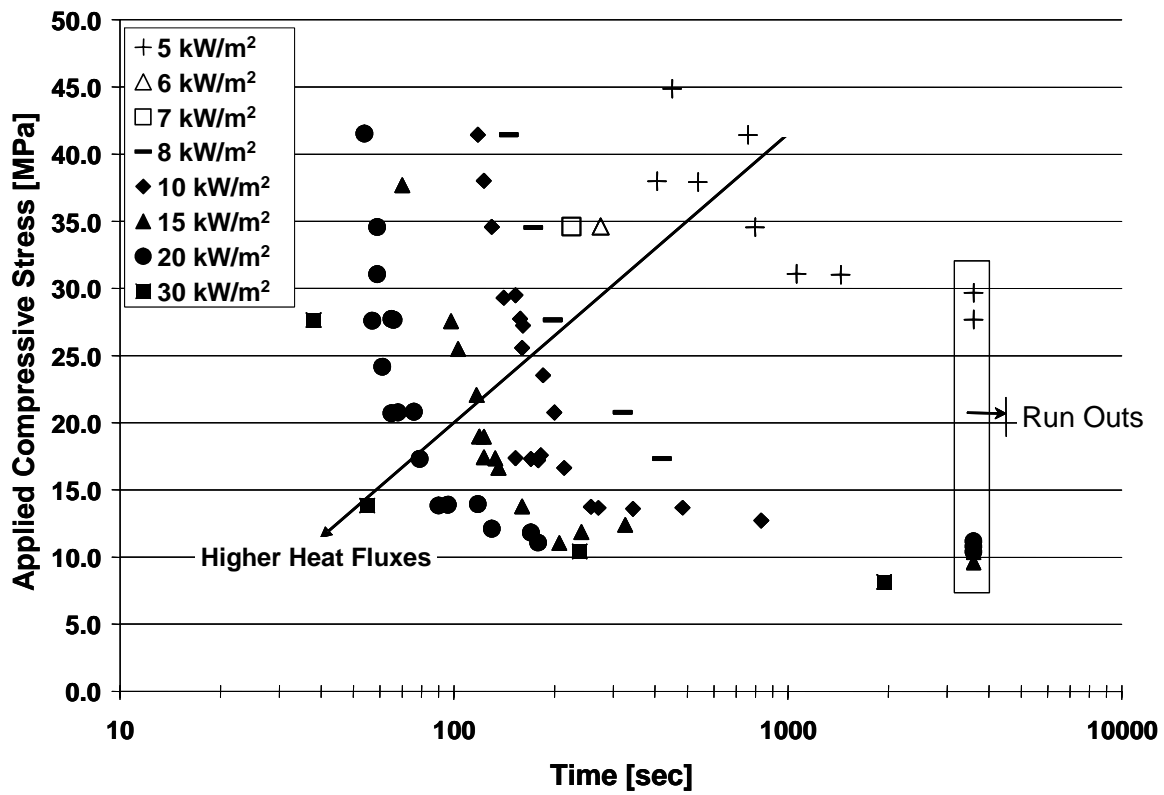


Figure 3-27: Times-To-Failure under Combined Loading

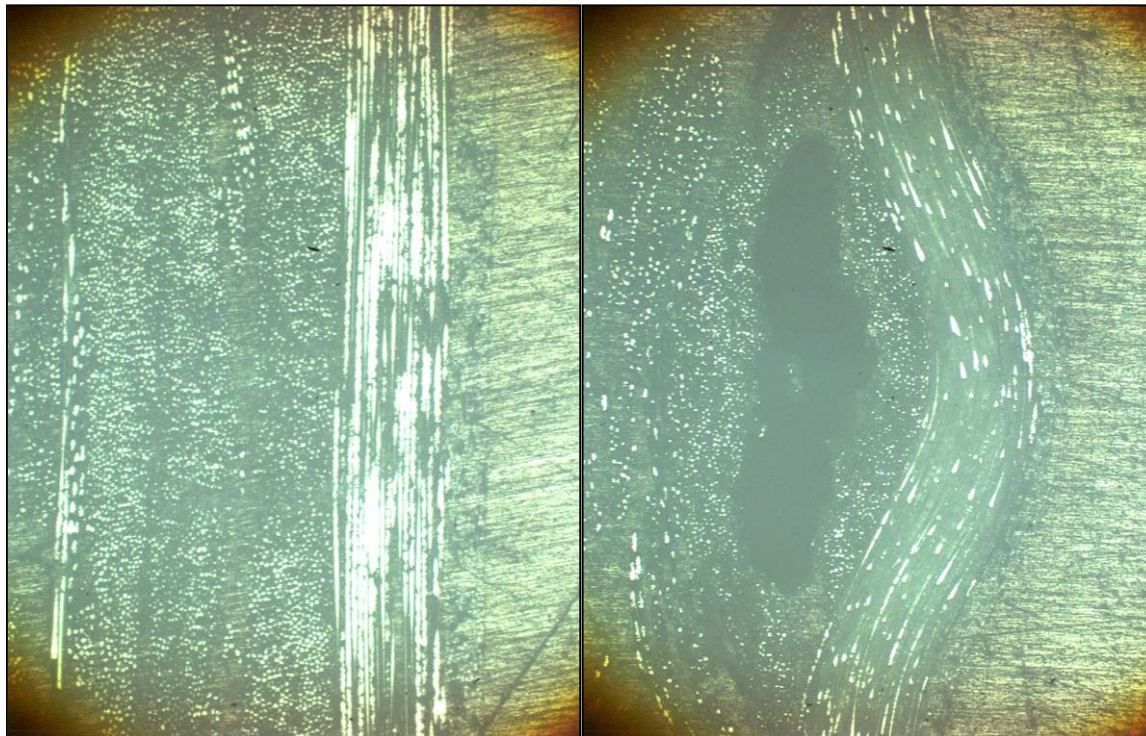
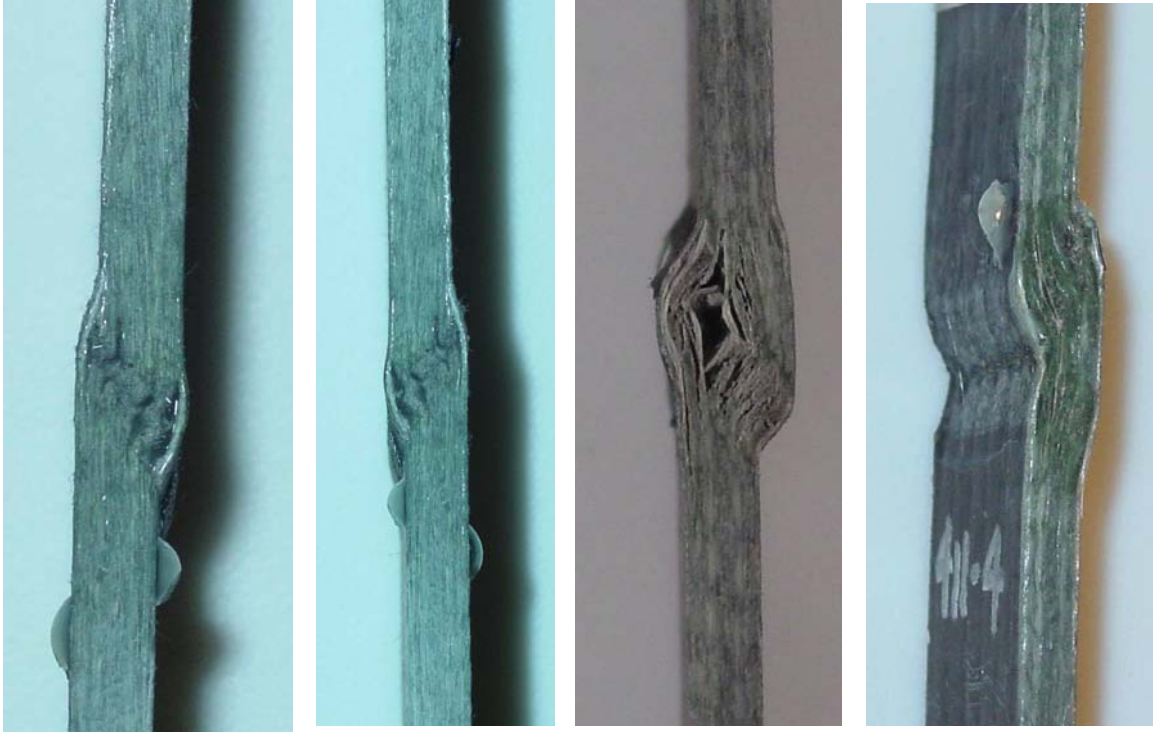


Figure 3-28: [0°] Ply Alignment Before and After Kinking



Mode 1

Mode 2

Mode 3

Mode 4

Figure 3-29: Compressive Failure Modes

CHAPTER 4 Analytical Development and Simulations

The prediction of the combined thermal and mechanical response of the laminates was performed in several steps. First the ply level thermal and mechanical properties must be determined. Then the temperature distribution through the thickness of the laminate, (i.e. on a ply level) was predicted over time for a specific heat flux. The predicted temperatures were used in a ply level stress analysis to determine the ply level stresses in the laminate. Failure of the laminate was determined through the comparison of the ply level stresses to predicted strength values given by the Budiansky and Fleck compression model. A flow chart summarizing the various steps in the overall simulation process is presented in Figure 4-1. The following sections describe in detail each step in the simulation.

4.1 Thermal Profile Models

4.1.1 Introduction

Prediction of the laminate temperature profiles through the thickness are required to solve for the thermal-mechanical response of PMC's exposed to a fire condition. Temperature profiles were determined using two methods, the first being a finite difference program written by the author and the second being a commercial finite element software package (ANSYS). Both simulations are capable of a variety of boundary conditions and able to account for the effect of changing material properties, as a function of temperature, (e.g. thermal conductivity and stiffness). The thermal analyses does not account for endothermic material degradation or mass transport effects.

4.1.2 Boundary Conditions

Within each simulation method, finite difference or finite element, two sets of boundary conditions were applied to determine the through the thickness temperature distribution as a function of time for a given heat flux.

4.1.2.1 Full Boundary Conditions

The first boundary condition set was termed "Full". This boundary condition set included heat transfer derived from convection, radiation and external heat flux. On the front

face (exposed to lamp) of the sample, heat transfer due to forced convection, radiation and absorbed external (lamp) heat flux were considered. On the back face only forced convection was considered.

During the experiments an exhaust fan was present on the front side (lamp side Figure 2-1) of the samples to remove fumes. This fan provided a forced convection boundary condition on the front side. The convection coefficients were assumed constant throughout time and over the entire exposed sample surface. The convection coefficients were estimated by fitting predicted front and back temperatures to average front and back temperatures collected from experiments. The convection coefficients varied for each heat flux and are listed in Table 4-1.

Table 4-1: Finite Difference Convection Coefficients

	5 kW/m ²	10 kW/m ²	15 kW/m ²	20 kW/m ²
Front Convection coefficient [W/m ² °C]	60	60	50	40
Back Convection coefficient [W/m ² °C]	60	50	40	30

The absorbed heat flux was not modeled as constant over time. When analyzing the heat flux data it was determined that the heat flux from the lamp required approximately four seconds to stabilize. This increase was linear and was modeled in this manner over the four second transient time.

4.1.2.2 Surface Temperature Boundary Conditions

The temperature profiles through the thickness were also determined using experimental surface temperature boundary conditions. Experimental front and back average temperatures computed for each heat flux level were applied as boundary conditions. This boundary condition set simplifies the task of determining the temperature.

4.2 Thermal Model Development

This section describes in detail the development of the finite difference program and the finite element model developed to predict the temperature profiles using the above discussed boundary conditions.

4.2.1 Finite Difference

The 1-D finite difference code was not extraordinary; other equivalent or superior (multidimensional) codes have been developed by many authors and were outlined in the above

literature review. The code was capable of taking into account the changing thermal properties as a function of temperature.

The heat transfer processes of convection, radiation and condition are governed by Equation (4-1) through (4-3). The energy balance for a discrete element on the front surface is given in Equation (4-4).

$$q''_{conv}(T_{surf}) = \bar{h}(T_{\infty} - T_{surf}) \quad (4-1)$$

where:

$$q''_{conv} = \text{Convection heat loss} \left[\frac{W}{m^2} \right]$$

$$\bar{h} = \text{Average Convection Coefficient} \left[\frac{W}{m^2 \text{ } ^\circ C} \right]$$

$$T_{surf} = \text{Temperature of Composite Surface} [^\circ C]$$

$$T_{\infty} = \text{Temperature of Surrounding Fluid} [^\circ C]$$

$$q''_{rad} = \varepsilon \sigma (T_{surr}^4 - T_{surf}^4) \quad (4-2)$$

where:

$$q''_{rad} = \text{radiation heat loss} \left[\frac{W}{m^2} \right]$$

$$\varepsilon = \text{Emmissivity}$$

$$\sigma = 5.67E-8 \left[\frac{W}{m^2 K^4} \right] (\text{Stefan Boltzman Consant})$$

$$T_{surf} = \text{Temperature of Composite Surface} [K]$$

$$T_{surr} = \text{Temperature of Surroundings} [K]$$

$$q''_{cond} = k \frac{dT}{dx} \quad (4-3)$$

where:

$$q''_{cond} = \text{Conduction Heat Loss} \left[\frac{W}{m^2} \right]$$

$$k = \text{Thermal Conductivity} \left[\frac{W}{m \text{ } ^\circ C} \right]$$

$$\frac{dT}{dx} = \text{Temperature Gradient} \left[\frac{^\circ C}{m} \right]$$

$$q''_{rad} + q''_{conv} + q''_{cond} + q''_{Lamp} = \rho c_p \frac{dT}{dt} \quad (4-4)$$

where:

$$q''_{Lamp} = \text{Absorbed Lamp Heat Flux} \left[\frac{W}{m^2} \right]$$

$$\rho = \text{Density} \left[\frac{kg}{m^3} \right]$$

$$c_p = \text{Specific Heat} \left[\frac{J}{kg \text{ } ^\circ C} \right]$$

$$dt = \text{Time rate of change of temperature} \left[\frac{^\circ C}{seconds} \right]$$

Equation (4-4) was solved using the Forward Euler time integration method. This is the most common definite difference method and is also known as the explicit time stepping method. This solution method is state forward in general. The sample was discretized into 11 nodes through the thickness. Nodes were placed on each face and at the mid-plane of each ply. A sufficiently small time step was chosen to assure convergence. The simulation was ran for each heat flux level and the resulting 1-D temperature distribution through the thickness of the laminate was saved for use as an input into the ply level thermal-mechanical stress analysis.

4.2.2 Finite Element

A transient thermal analysis was conducted in ANSYS ® Multiphysics™ 7.0 to predict the temperature distribution throughout the samples over time. The FEA model constructed used an eight node three dimensional thermal element with one degree of freedom (temperature) at each node. There were nine elements through the thickness of the model, and each element was the thickness of one ply. The FEA model was 100 mm long, with 50 mm exposed to the temperature boundary conditions simulating the area of the heat flux exposure, Figure 4-2. The grip area of the specimens was set as perfectly insulated. The model was then solved for each boundary condition set and each applied heat flux, the results were saved for later use in the thermal-mechanical modeling.

4.3 Mechanical Models

4.3.1 Introduction

The temperature profiles were used as inputs into a thermal-mechanical stress analysis in an effort to determine the ply level stresses and deformations over time. The temperature profiles were used to evolve the mechanical properties of the off axis plies as a function of temperature. The off axis stiffness of the laminate is highly dependent upon temperature, as shown in Figure 3-6. Therefore the temperature distribution leads to a stiffness distribution through the thickness that must be computed in order to determine the ply level stresses.

Two methods were used for predicting the mechanical responses of these composites at elevated temperatures while under applied compressive loads. The first was Classic Laminate Theory analysis (CLT) and the second was a finite element analysis using ANSYS. In both analyses failure was said to occur when the ply level stress was greater than that of the temperature dependent Budiansky & Fleck compression strength. Details on the general inputs into the mechanical simulation, Budiansky & Fleck [32] compression model, CLT program and FEA simulation are presented below in more detail.

Using both analysis methods, predictions of failures times, and sample deformations were compared to experimental results in an effort to determine the accuracy of each model.

4.3.2 Temperature Profiles Used

Temperature profiles are the foundation for the mechanical analysis because the off axis elastic properties are strongly influenced by temperature. Thus, the through the thickness temperature profiles are used as input to the thermal-mechanical CLT and FEA analyses. The surface temperature boundary condition results were used instead of the full boundary conditions because they more accurately represent the temperature profiles of the experimental conditions.

4.3.3 Mechanical Material Properties as a Function of Temperature

Again, the off axis ply properties are a strong function of temperature. The $E_{22}(T)$ stiffness used in the analysis is consistent with that determined experimentally and presented in section 3.3. The in-plane shear modulus, G_{12} was also evolved as a function of temperature and detailed below. E_{11} , ν_{12} , α_{11} and α_{22} were all held constant over the temperature range

investigated. In actuality, these properties are most likely dependent on temperature (albeit, not as strongly dependent as G_{12} and E_{22}).

4.3.4 Modified CLT

A modified CLT program was developed that takes into account a non-uniform temperature profile through the specimen thickness and allows for plywise temperature dependent mechanical properties. The analysis begins by applying a constant mechanical load. Looping through the temperature input files calculating the ply level stresses and strains at each time step. This mechanical analysis is coupled with the temperature dependent Budiansky & Fleck failure criteria. For each time step the ply level stresses of both $[0^\circ]$ plies were compared to the failure criteria in order to determine the time to failure. The failure times of each ply were determined for a variety of mechanical loading cases (i.e. heat flux & compression load). Total sample failure was said to occur when both $[0^\circ]$ plies of the quasi-isotropic laminate failed.

4.3.5 Mechanical Finite Element Analysis

The FEA thermal-mechanical model was based on the same geometry as the thermal model discussed above. The thermal elements were modified using an ANSYS command from three dimensional thermal elements to three dimensional solid elements. The size and location of each element remained the same, only the element type changed to Element 45, a linear eight node three dimensional structural element. The analysis method employed the temperature results from the FEA thermal model as body loads for the mechanical model.

The mechanical constraints on the model are illustrated in Figure 4-2. The orientation of the model has the Y-axis along the length, the Z-axis through the thickness and the remaining X-axis is in the direction of width of the sample. At the lower grip section, the lowest 25 [mm] on either side of the model, the x, y, and z displacement constraints were set to zero. At the top grip section, the top most 25 [mm] front and back of the model, the x and z displacements were set to zero, but was allowed to move vertically in the y axis. A pressure was applied to the upper edge of the model representing the applied mechanical load. These boundary conditions were an attempt at modeling the constraints the grips of the testing frame applied to the sample.

Instead of using a transient mechanical analysis, consecutive static analyses were performed to predict the plywise stress over time where ply level stiffnesses are evolved as a result of the changes in through the thickness temperature profile. For every time step the

displacement constraints and the specified pressure are held constant but the nodal temperatures are modified to match those of the thermal results. These temperatures were previously determined from the thermal analysis for every node in the model. The FEA mechanical analysis also used the temperature dependent Budiansky-Fleck failure criteria. Total sample failure was said to occur when both $[0^\circ]$ plies of the quasi-isotropic laminate failed.

The displacements determined from the FEA analysis were calculated so as to reproduce the laser extensometer readings used in the experimental study. As the sample is heated during testing bending occurs, however the laser extensometer does not sense the bending strain. Instead, the laser only measured the vertical displacement of the reference lines, again the reference lines were 45mm apart. In an effort to reproduce that reading, the vertical component of the nodal translation was recorded for two nodes, one near the upper and lower near the lower grip of the model. These purely vertical displacements were then converted into an overall specimen strain which could be compared to the strains recorded by the laser extensometer.

4.3.6 Budiansky and Fleck Failure Criteria

After the discovery that failure was dominated by a kink band formation failure, a failure criteria had to be chosen that could adequately capture such phenomena. The Budiansky and Fleck model describes the elastic-plastic kink formation in unidirectional laminates. The description of the kink formation also includes the shear response of the matrix and the initial misalignment of the fibers, Figure 4-3 shows a schematic of this phenomenon. Equation (4-5) is the Budiansky & Fleck failure criteria equation used to determine the stress required to failure a $[0^\circ]$ ply.

$$\sigma_{compression} = G_{12} \left[1 + n \left(\frac{3}{7} \right)^{\frac{1}{n}} \left(\frac{\bar{\phi}}{\gamma_Y (n-1)} \right)^{\frac{n-1}{n}} \right]^{-1} \quad (4-5)$$

where:

$\sigma_{compression}$ = Coomprssive Strength [Psi]

G_{12} = Shear Modulus [Psi]

n = Strain Hardening Index

$\bar{\phi}$ = Initial Fiber Misalignment

γ_Y = Yeild Shear Strain [in / in]

The strain hardening index is a material parameter that is determined from experimental data using Equation (4-6) which is the Ramberg/Osgood shear stress – shear strain relationship.

$$\frac{\gamma}{\gamma_Y} = \frac{\tau}{\tau_Y} + \left(\frac{3}{7}\right) \left(\frac{\tau}{\tau_Y}\right)^n \quad (4-6)$$

where:

$$\frac{\gamma}{\gamma_Y} = \frac{\tau}{\tau_Y} + \left(\frac{3}{7}\right) \left(\frac{\tau}{\tau_Y}\right)^n$$

$\gamma = \text{Shear Strain}[in / in]$
 $\gamma_Y = \text{Yield Shear Strain}[in / in]$
 $\tau = \text{Shear Stress}[Psi]$
 $\tau_Y = \text{Yield Shear Stress}[Psi]$
 $n = \text{Strain Hardening Index}$

Shear properties of a similar glass/vinyl ester composite was determined by Phifer [30]. The resulting shear stress strain plot is reproduced in Figure 4-4. From this plot the shear modulus, yield shear strain and yield shear stress were calculated at , 25, 50 and 95°C. The shear modulus is plotted as a function of temperature in Figure 4-5, and the yield shear properties are given in plotted in Figure 4-6. Using the data the Ramberg-Osgood strain hardening index was determined to be 3.5, and was found to be independent of temperature. Using a fiber undulation angle of 7° degrees the Budiansky and Fleck compression strength was calculated as a function of temperature and is plotted in Figure 4-7. To emphasize the correlation between shear stiffness and compression strength the shear modulus and compression strength were normalized by their respective values at 25°C and plotted as a function of temperature in Figure 4-8.

4.4 Figures

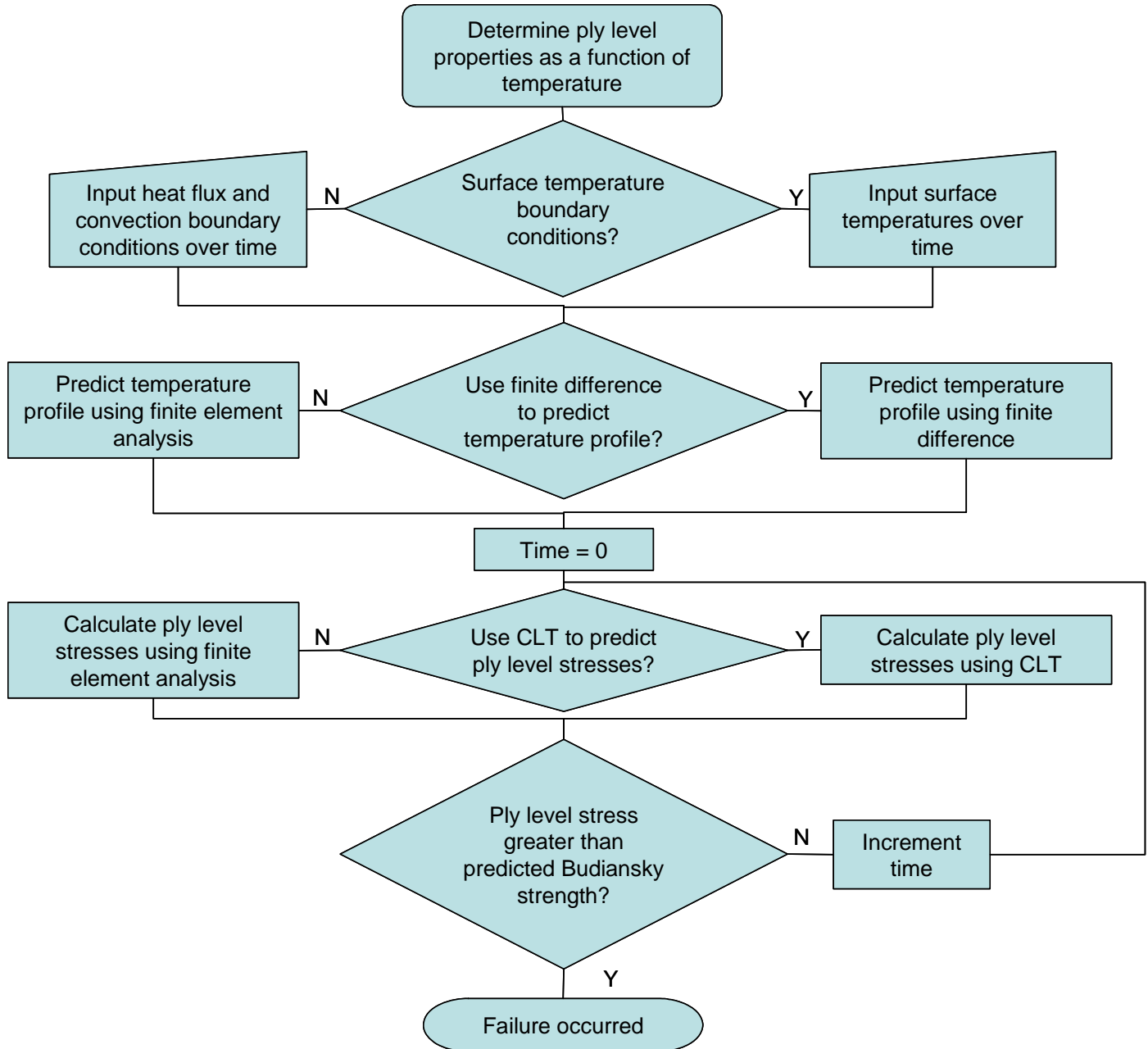


Figure 4-1: Simulation flow chart

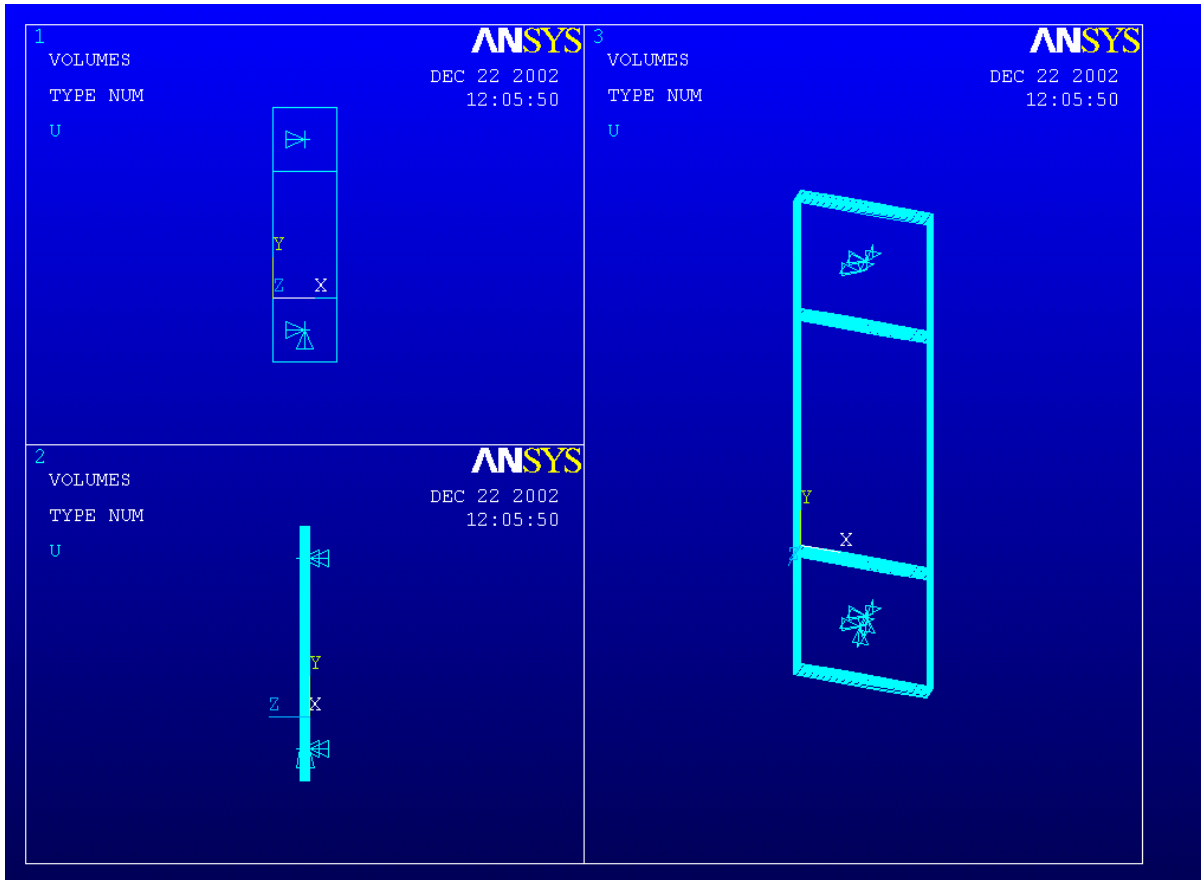


Figure 4-2: FEA Model

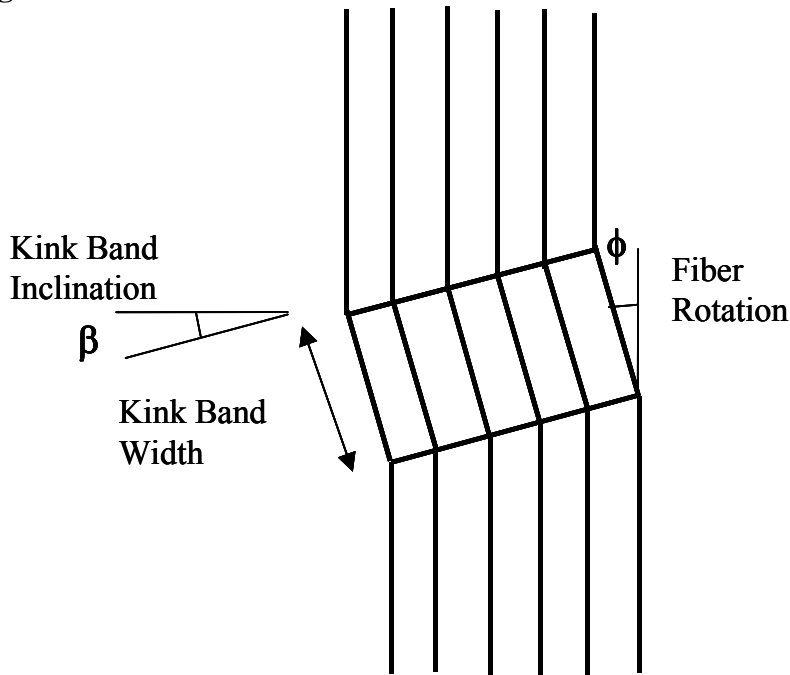


Figure 4-3: Budiansky & Fleck Kink Band Schematic

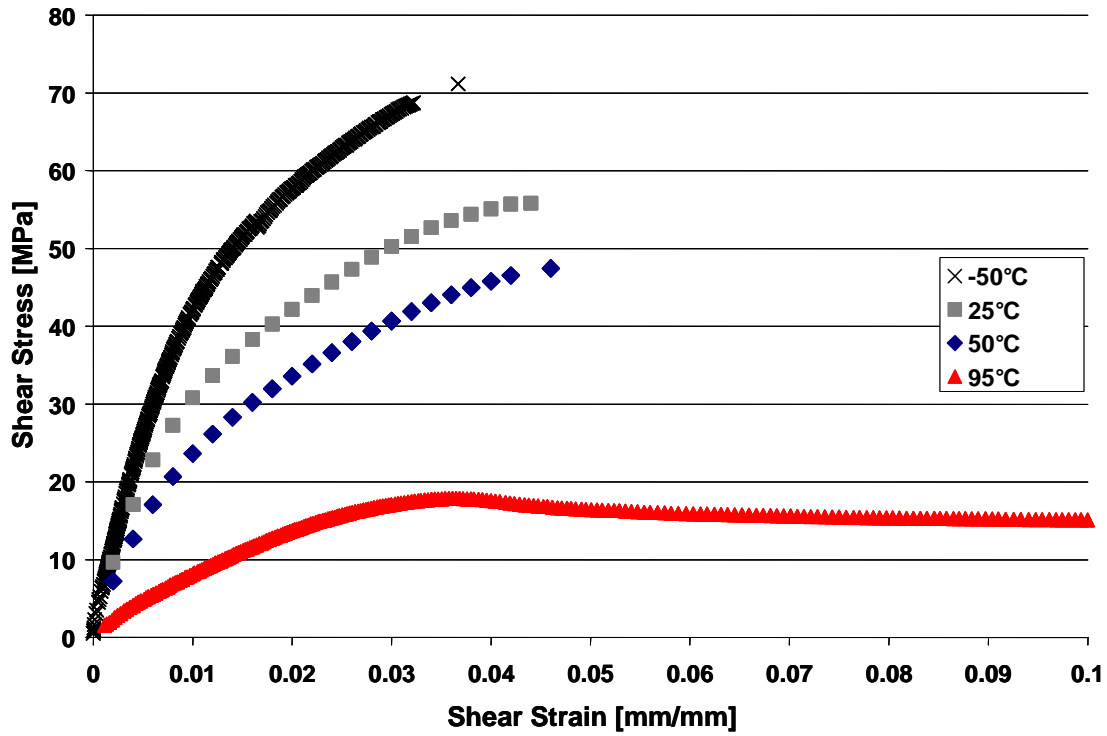


Figure 4-4: Shear Stress – Strain Properties of Glass/Vinyl Ester [+45°] Laminates

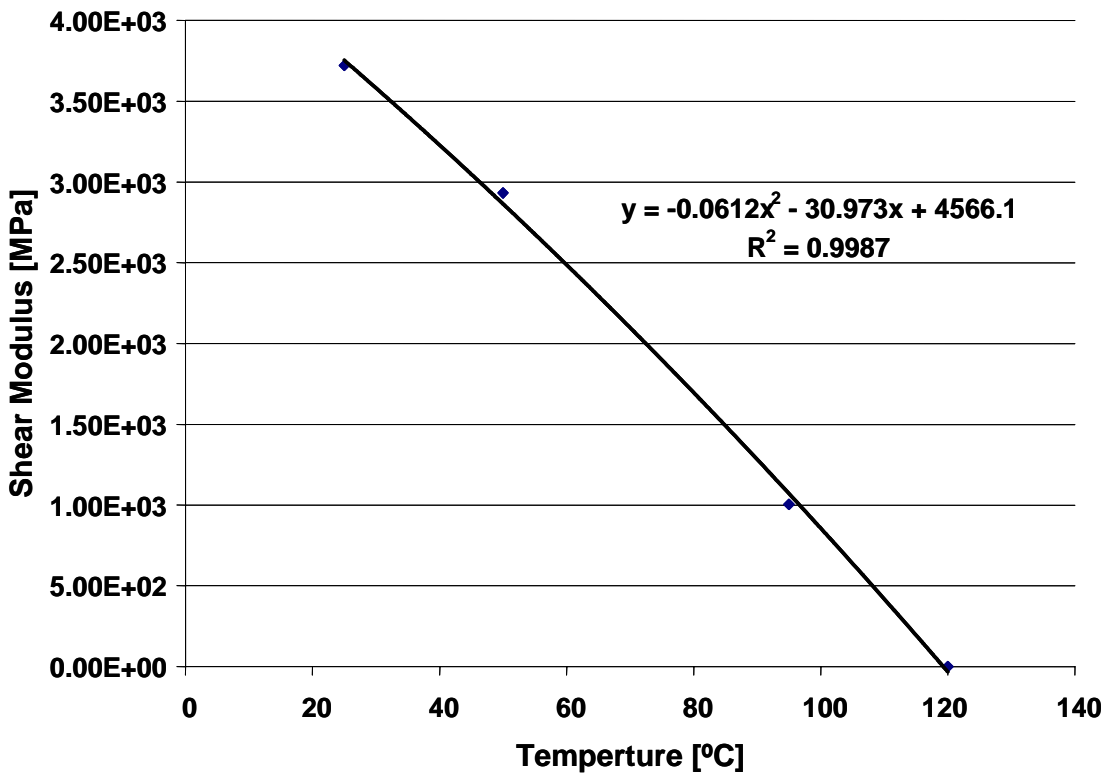


Figure 4-5: Shear Moduli of Glass/Vinyl Ester [+45°] Laminates

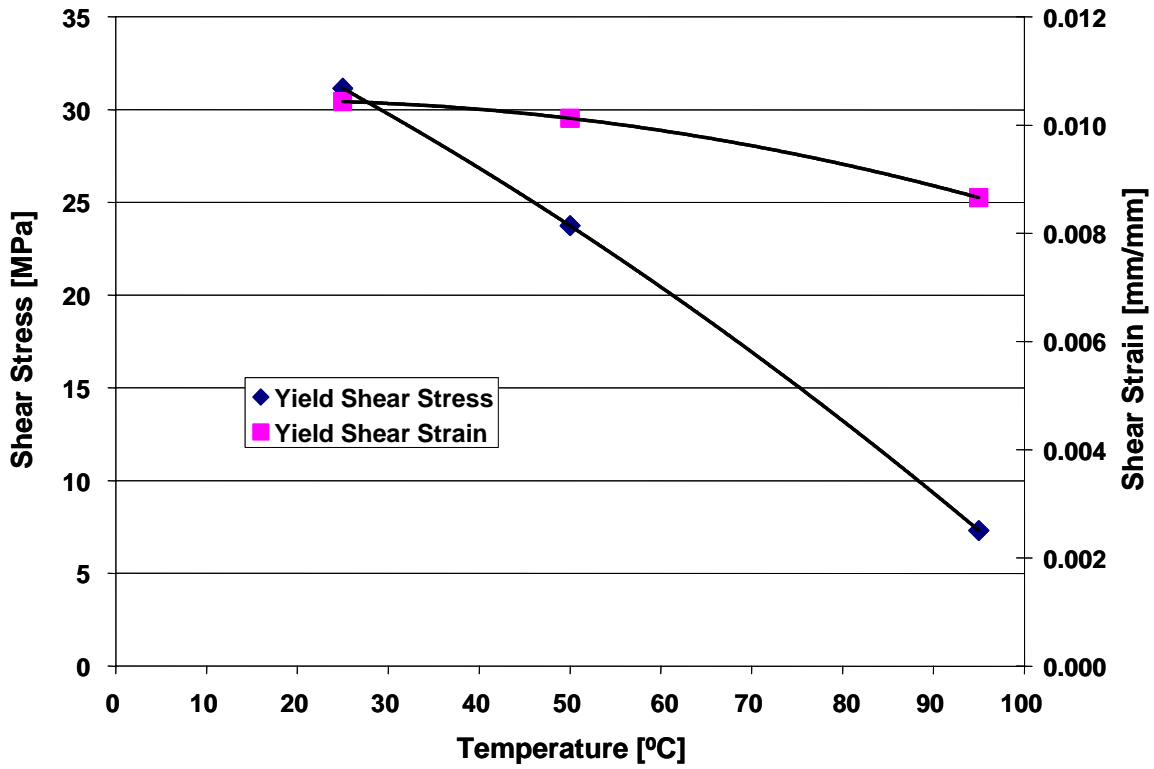


Figure 4-6: Shear Yield Properties

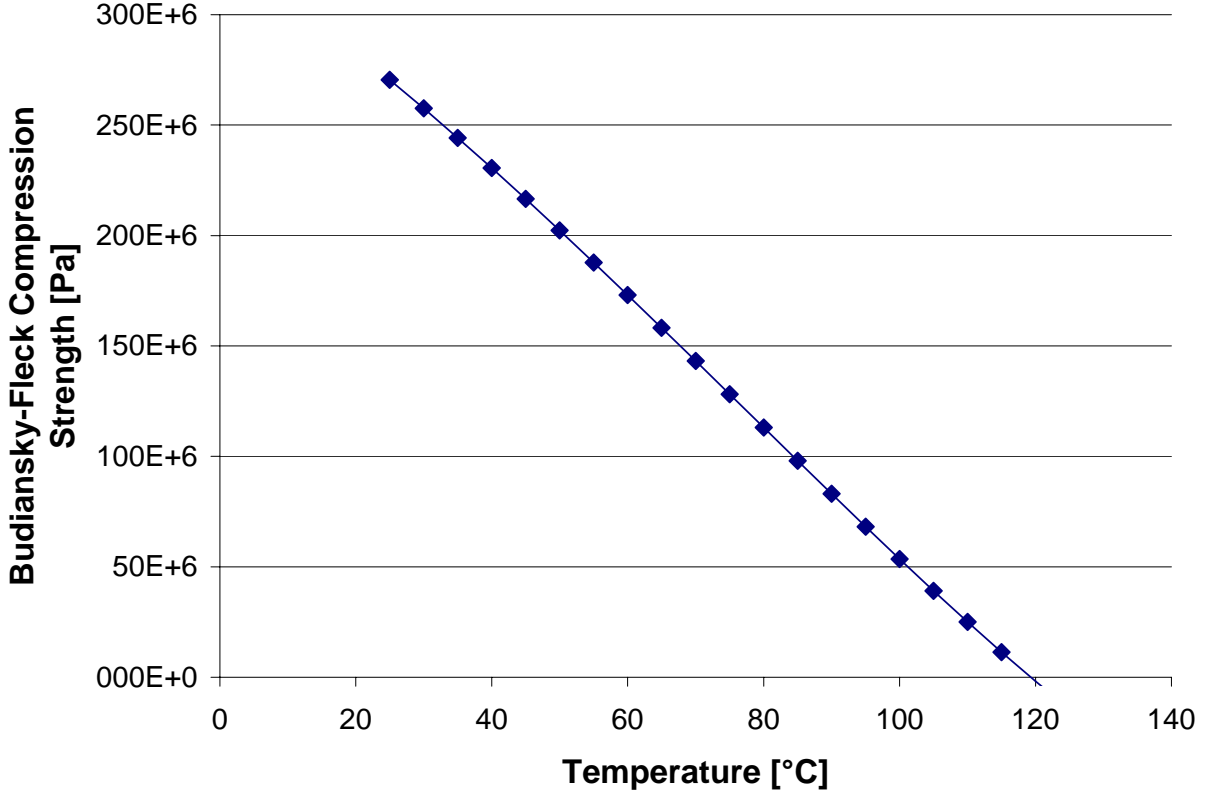


Figure 4-7: Budiansky-Fleck Compression Strength vs. Temperature

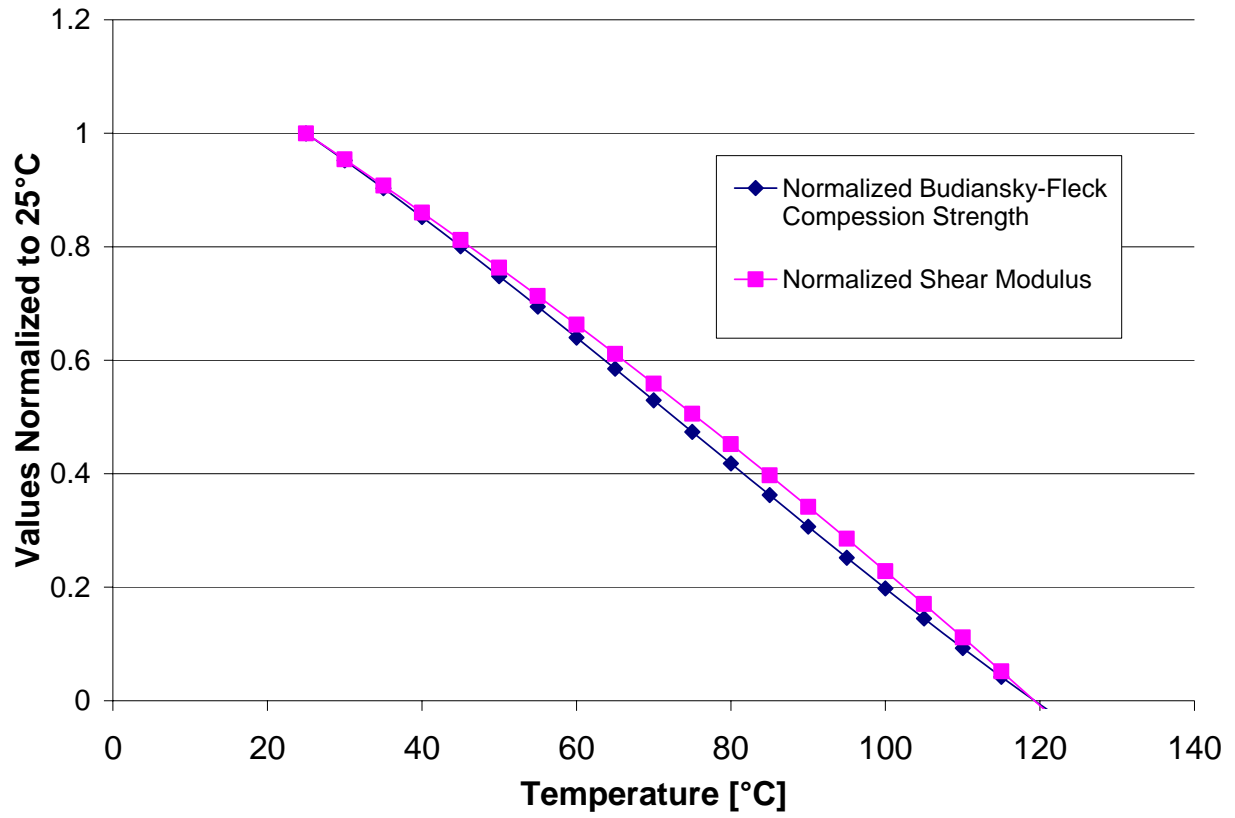


Figure 4-8: Normalized Shear Modulus and Compression Strength vs. Temperature

CHAPTER 5 Analytical Results Compared to Experimental Data

5.1 Laminate Thermal Response

The thermal response of the laminate was predicted, as previously described, and the results are discussed below. Predicted surface temperatures will be presented and compared to experimental data. Unfortunately there is no intra laminar temperature data to compare the predicted through thickness temperatures against.

5.1.1 Finite Difference Temperature Results and Comparisons

In Figures 5-1 through Figure 5-4 the predicted front and back temperature profiles are presented for the 5, 10, 15 and 20 [kW/m²] input heat fluxes, along with the average recorded front and back temperatures. The predicted face temperatures are consistently hotter than the recorded average, but are considered to be a good fit to the data.

Sources of error for the calculation could result from convection boundary conditions that were used. Both front and back coefficients were assumed constant, in reality they are not. The coefficients will increase as the sample temperature increases. Moreover the thermal diffusivity for the glass – vinyl ester as a function of temperature is estimated from data on carbon – phenolic epoxy data.

The through the thickness temperature prediction is plotted in Figure 5-5 as a contour plot. Each color band represents a 10°C temperature range. The x-axis is time in seconds and the y-axis is the ply interface number, zero and 9 being the exposed front and back plies respectively. The significance of this plot is the conformation of the high temperature gradients in the sample. As an example for an applied 20 [kW/m²] at 100 seconds there are nine temperature bands through the thickness of the sample. That corresponds to a 90°C temperature gradient front to back. As the heat flux is increased the induced thermal gradient is also increased.

5.2 Mechanical Responses

The strain profile predictions and times to failure are predicted for a variety of thermal and mechanical loading cases. The results are presented, compared with predictions and discussed.

5.2.1 Time to Failure Predictions

The results for the time to failure predictions agree very well with experimental data for high mechanical loads and high heat fluxes. The results of the 20 [kW/m²] failure predictions for both CLT and FEA analysis along with the collected experimental data are shown in Figure 5-6. The triangle symbols correspond to the front [0°] ply failure times while the squares correspond to the back [0°] ply failure time. Both CLT and FEA predictions for time to failure show reasonable agreement with the data at the higher mechanical loads. However, for compressive loads less than 14 [MPa] the predictions deviate considerably. The prediction accuracy at the higher mechanical loads is also observed for the 10 and 15 [kW/m²] heat fluxes (Figure 5-7, Figure 5-8). Generally good agreement in failure times occurs at compressive stresses above the 14 [MPa]. Below this threshold the predicted failure times are considerably quicker than the collected data. At the 5 [kW/m²] heat flux level only the front [0°] ply failures were predicted, hence no specimen failure was predicted at this heat flux level. Referring back to Figure 3-9 it should be noted that thermal equilibrium occurs at approximately 400 seconds, and the minimum time to failure for a sample that was tested at 5 [kW/m²] was 450 seconds. This means that all samples tested at this heat flux had attained and sustained thermal equilibrium for some period of time. Some samples survived thermal equilibrium for 1000 seconds before failing. This leads to the conclusion that the samples are not failing due to thermal effects alone, but are failing due to a combination of thermal and viscoelastic effects.

At load levels significantly higher than that of the run out stress the predicted times to failures were longer than experimental data. Again, the elevated temperature creep of this composite was not considered in this study. If creep were to be included the predicted failure times would be quicker. This would bring the predicted times to failures at higher load levels into better agreement with the experimental data.

5.2.2 Strain Profile Predictions

Four representative predicted axial strain profiles are plotted in Figures 5-10 through Figure 5-13. A typical prediction of the strain as a function of time from both the CLT and FEA approaches is shown in Figure 5-12, for the case of 15 kW/m^2 and an applied compressive stress of 27.5 MPa . Note that the initial positive slope is a strong function of thermal expansion and represented relatively well by the FEA model as the true boundary conditions are more closely represented than that accomplished in the CLT point stress analysis. Thus, the apparent bending of the specimen due to thermal gradient plays a role in the response of the laminate stresses. However, when comparing the times at which the front and back 0° plies fail (solid symbols within the strain predictions), the lives are relatively close. Complete failure of the laminate is expected after both front and back unidirectional plies have failed (in this case about 110 seconds).

In addition it should be noted that after the strain reaches the maximum, both analyses cease to predict the strain accurately. The actual strain from experiment decreases at a faster rate than is predicted with FEA or CLT. This behavior is most likely due to the buckling of the front 0° ply and the fact that no additional efforts are made to calculate the effect of this local loss in the subsequent stress redistribution. Despite these shortcomings, there is reasonable agreement between the predicted the time to failure of the laminates under these combined conditions and the experimentally observed times. The predictions for a heat flux of 20 kW/m^2 show good agreement up to about 13 MPa where the observations begin to exceed the predictions (Figure 5-6). Also note that for both the CLT and FEA analysis there is good agreement between the predictions for assessing the front and back face 0° plies. Similar trends are noted for 15 kW/m^2 . However, as we approach lower heat flux levels the model begins to deviate as anticipated with the predictions showing longer lives than that observed, as shown in Figure 5-7. We suggest that this is due to the absence of the creep effects in the modeling, which would tend to reduce the life. At 5 kW/m^2 we are not able to predict failure of the laminates as we believe that life under these conditions is controlled by creep and not just the effects of stiffness changes as the glass transition is approached.

5.3 Figures

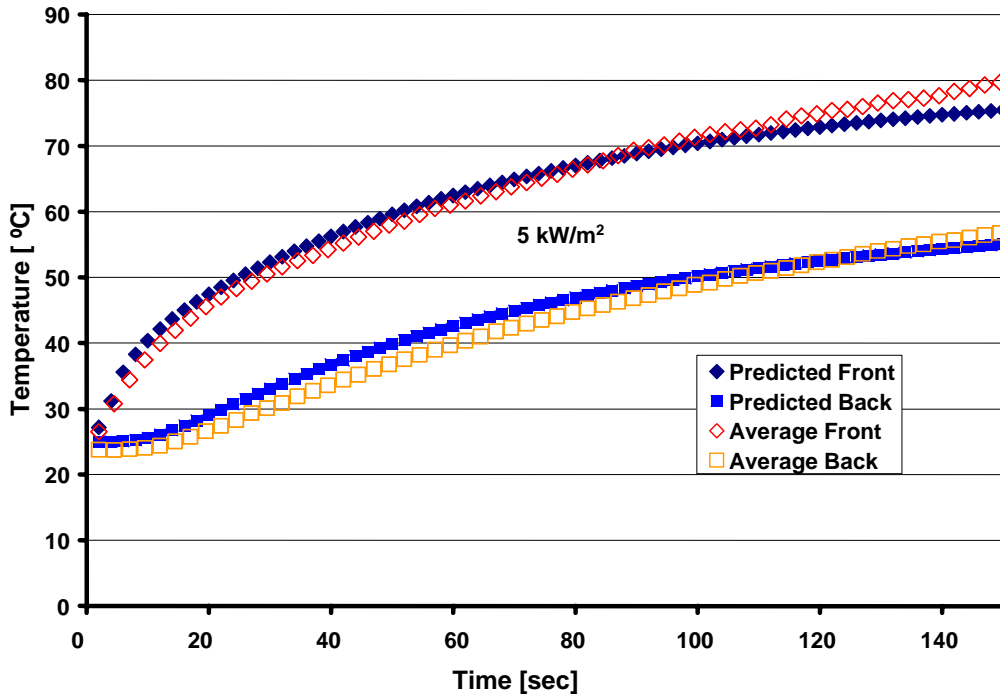


Figure 5-1: 5 kW/m² Temperature Profile Results vs. Collected Data

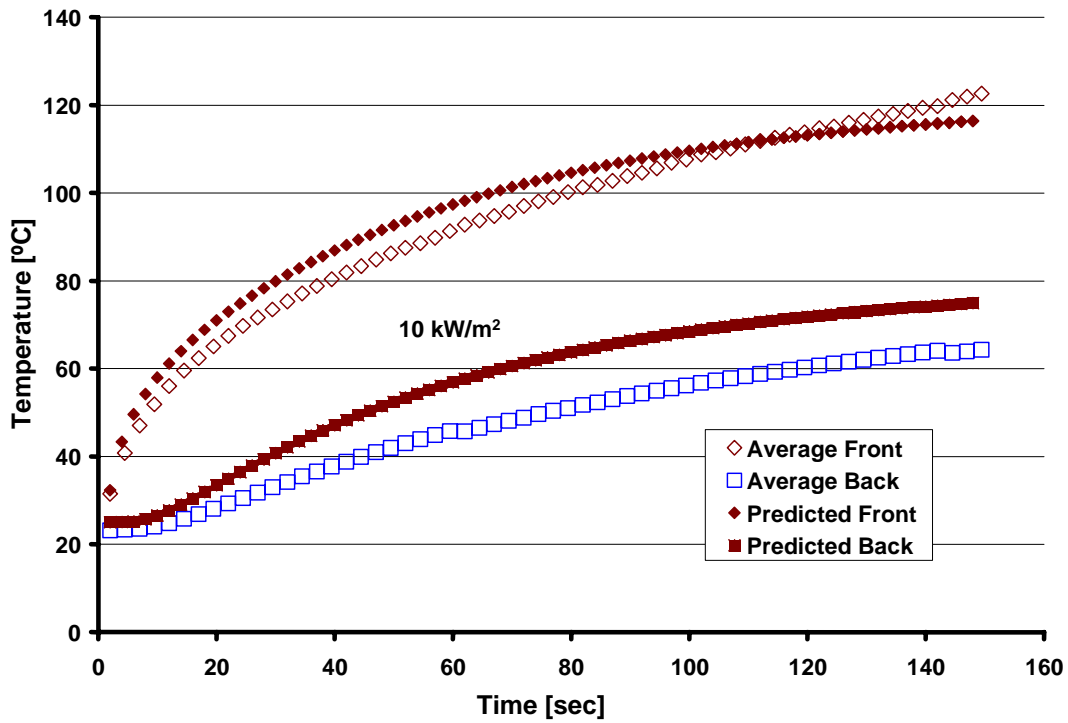


Figure 5-2: 10 kW/m² Temperature Profile Results vs. Collected Data

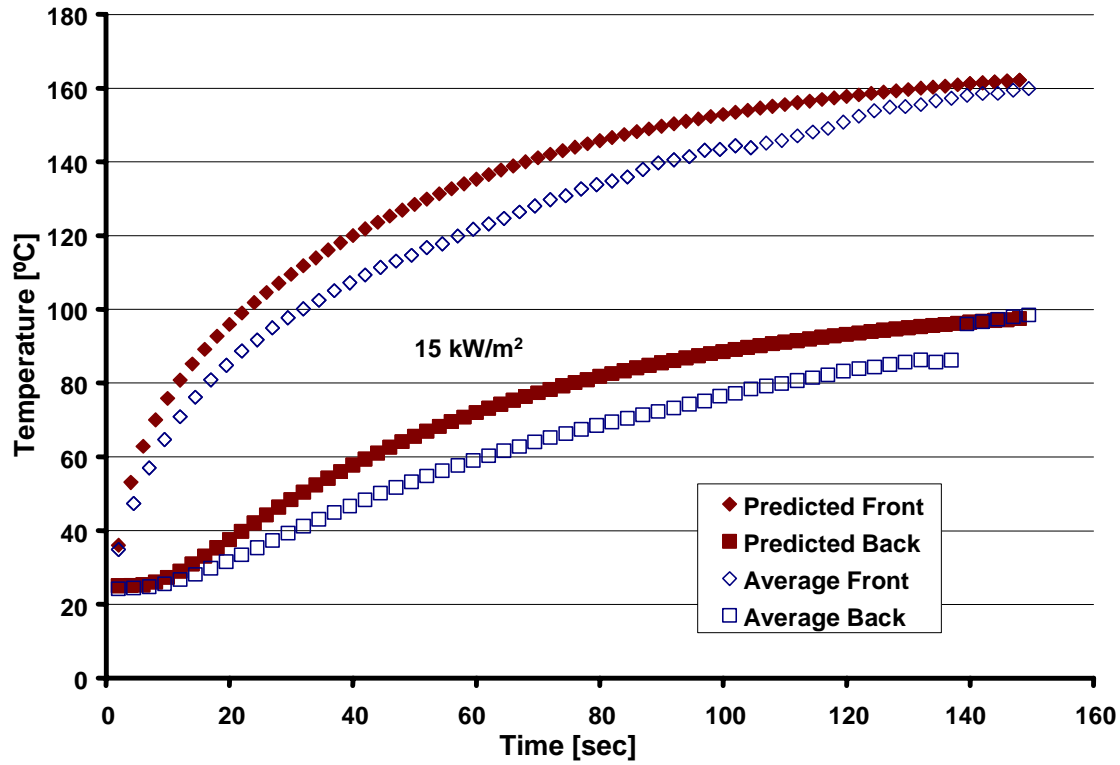


Figure 5-3: 15 kW/m² Temperature Profile Results vs. Collected Data

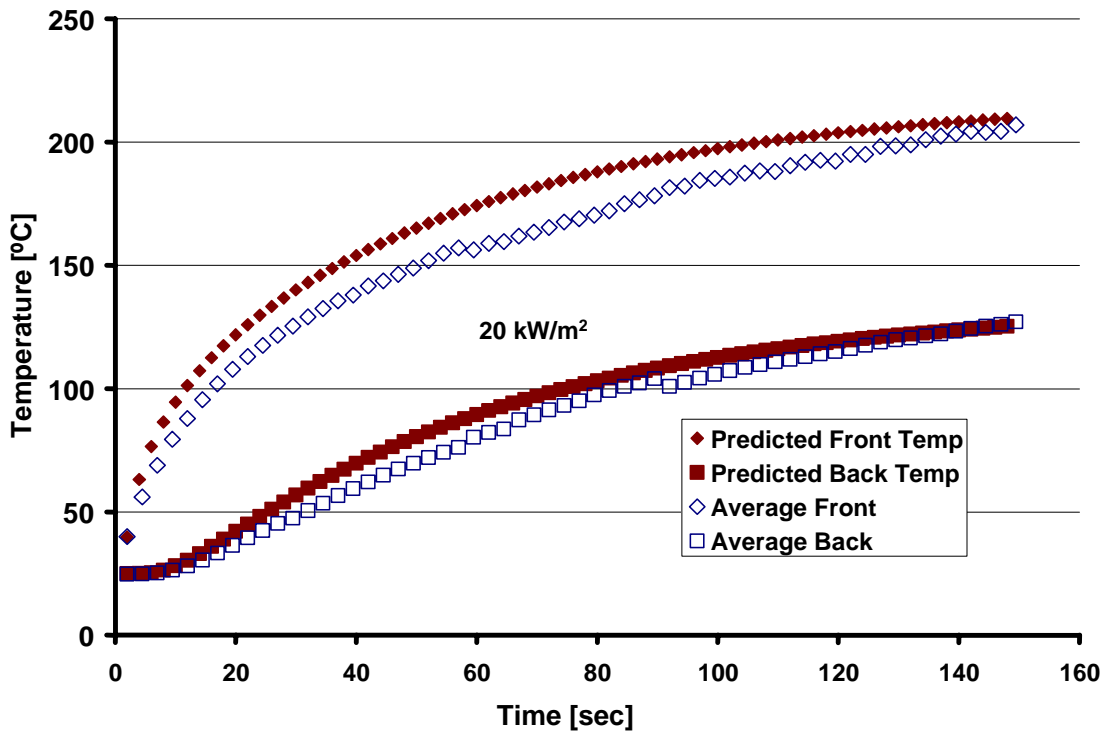


Figure 5-4: 20 kW/m² Temperature Profile Results vs. Collected Data

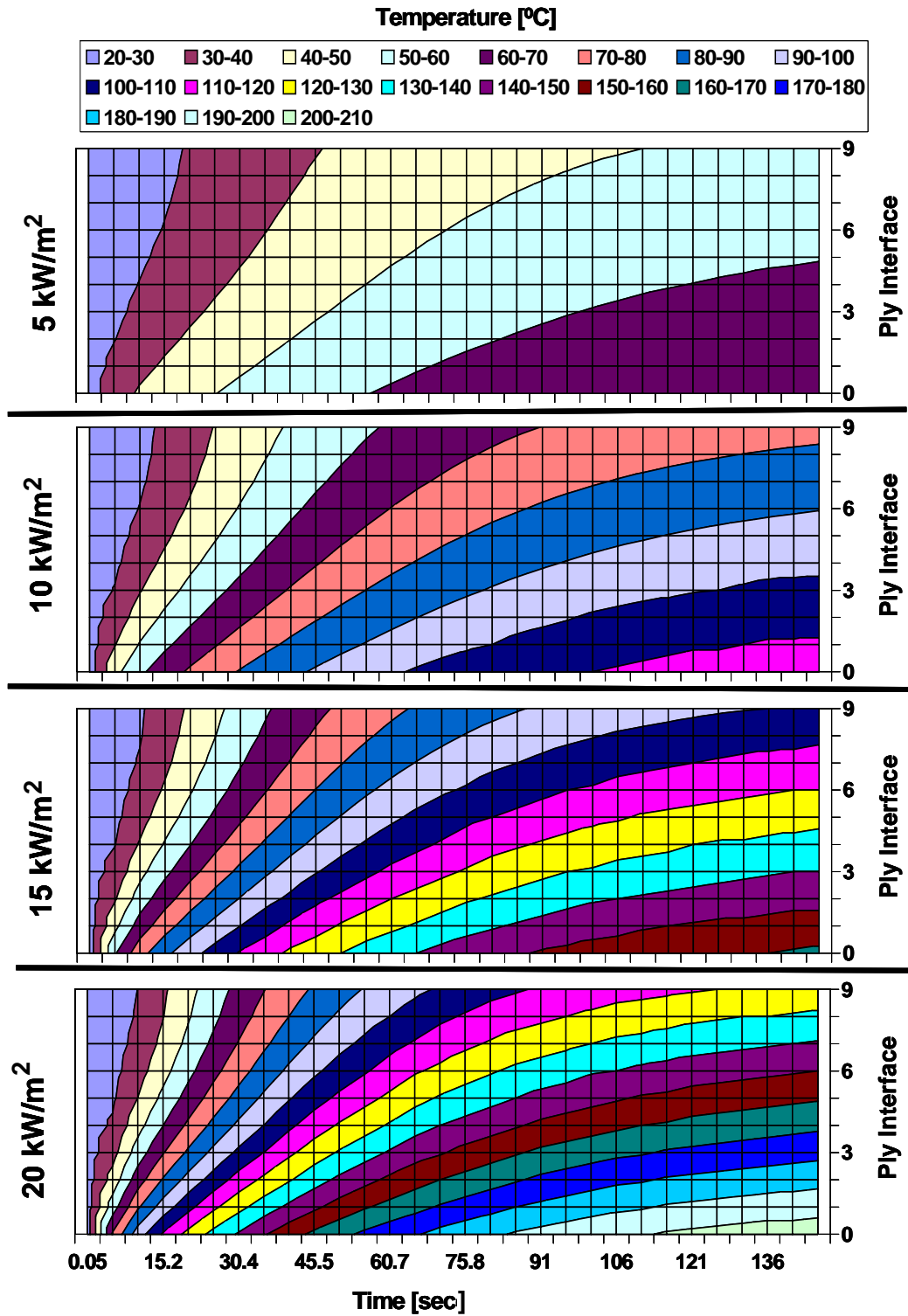


Figure 5-5: Through the Thickness Temperature Perditions

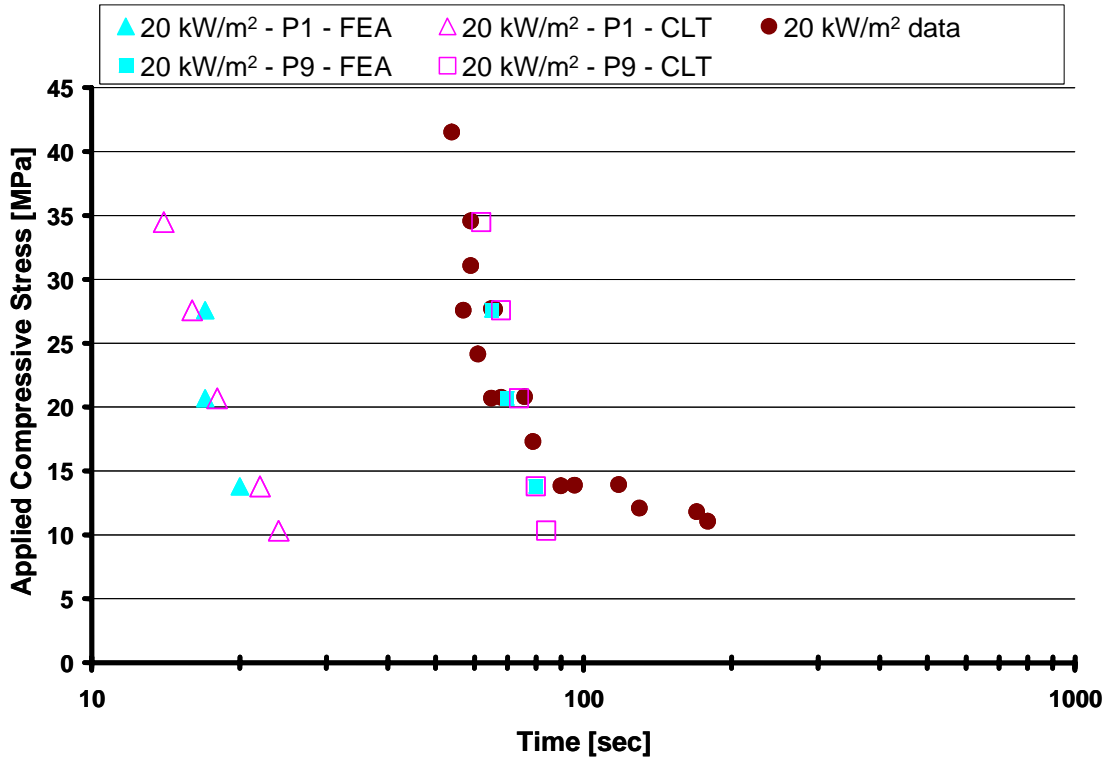


Figure 5-6: 20 kW/m² Time to Failure Predictions

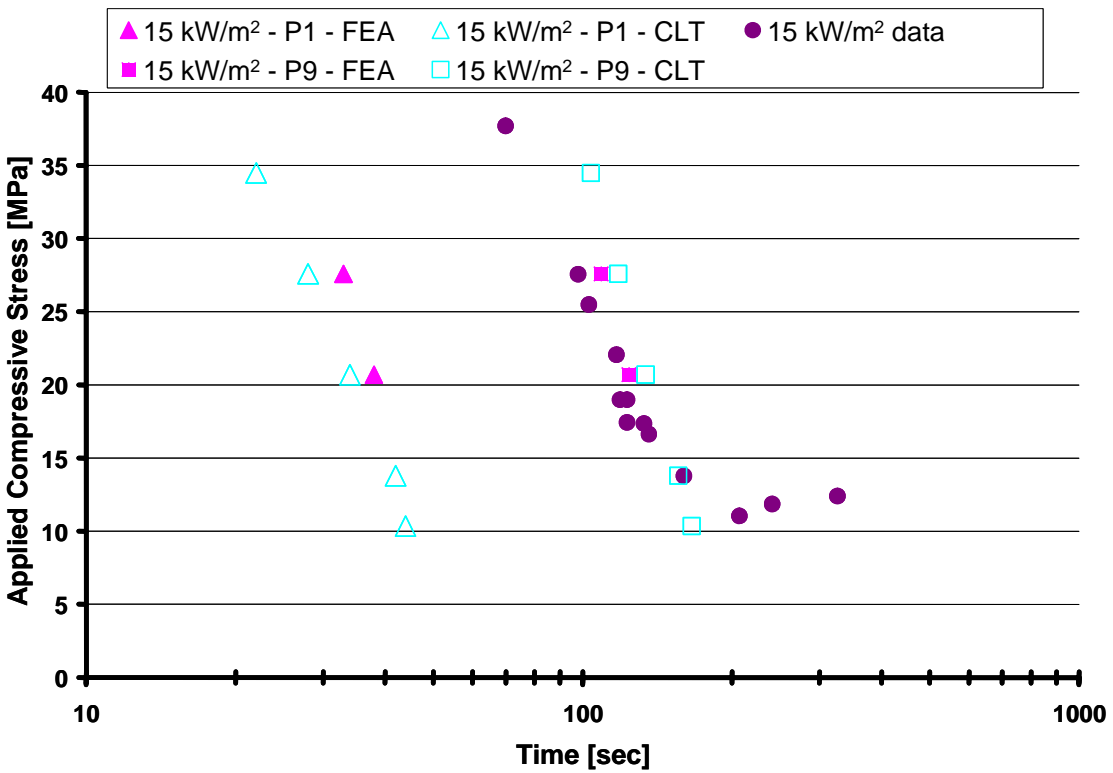


Figure 5-7: 15 kW/m² Time to Failure Predictions

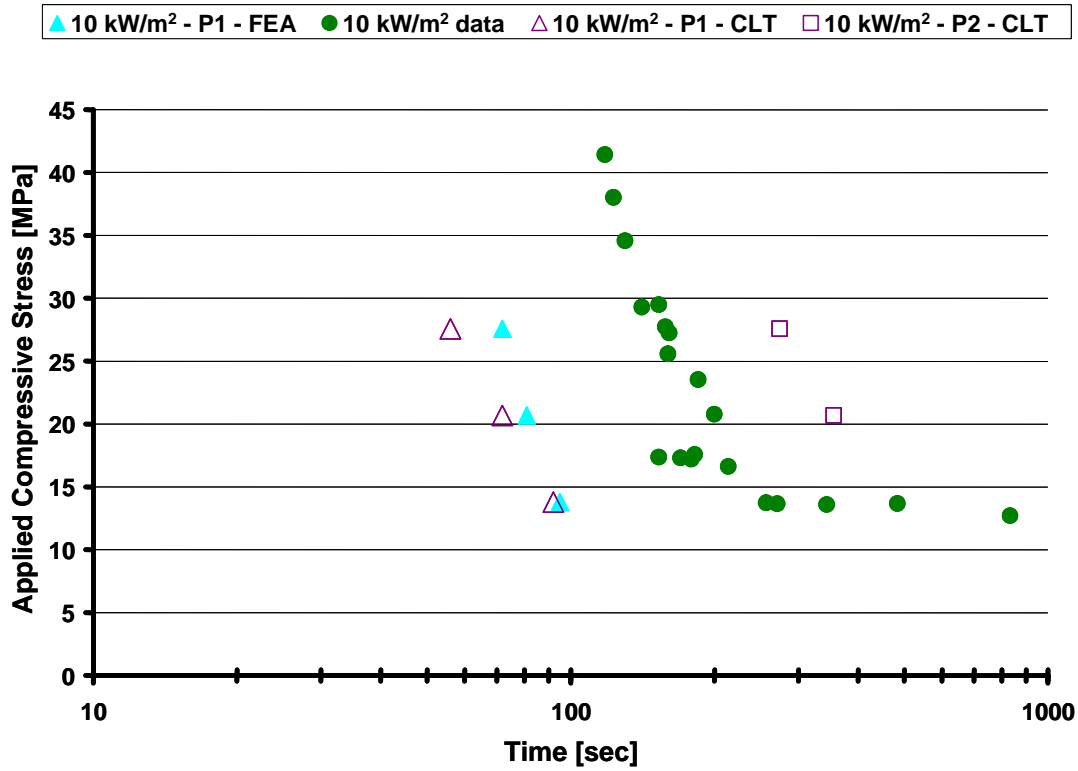


Figure 5-8: 10 kW/m² Time to Failure Predictions

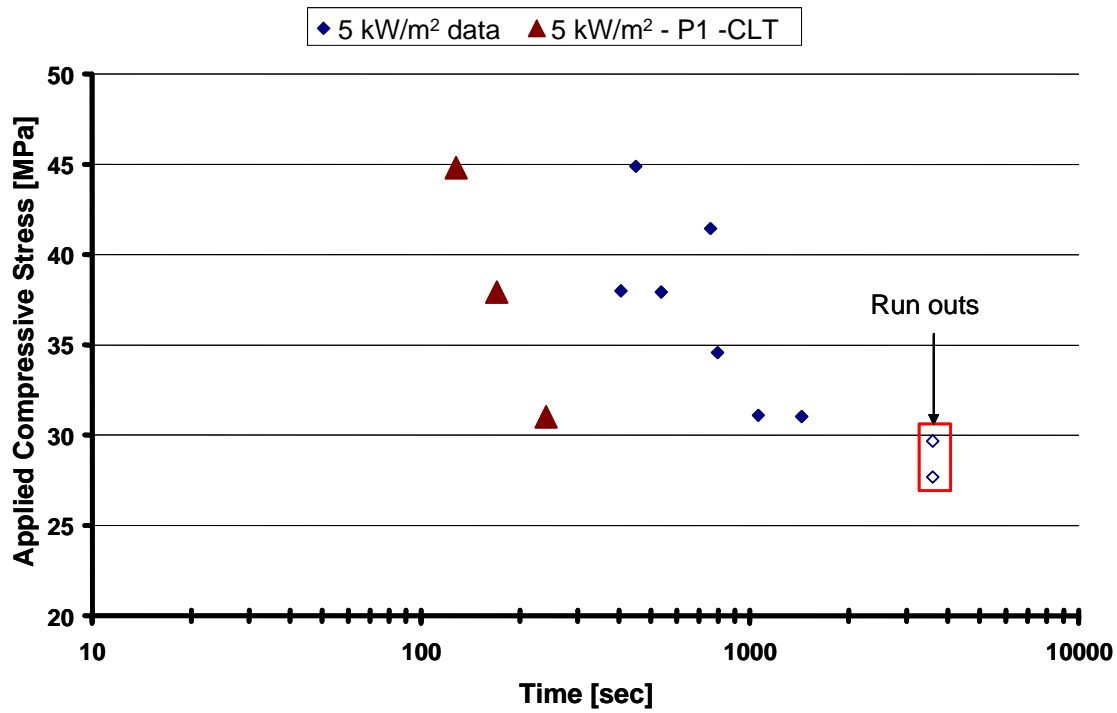


Figure 5-9: 5 kW/m² Time to Failure Predictions

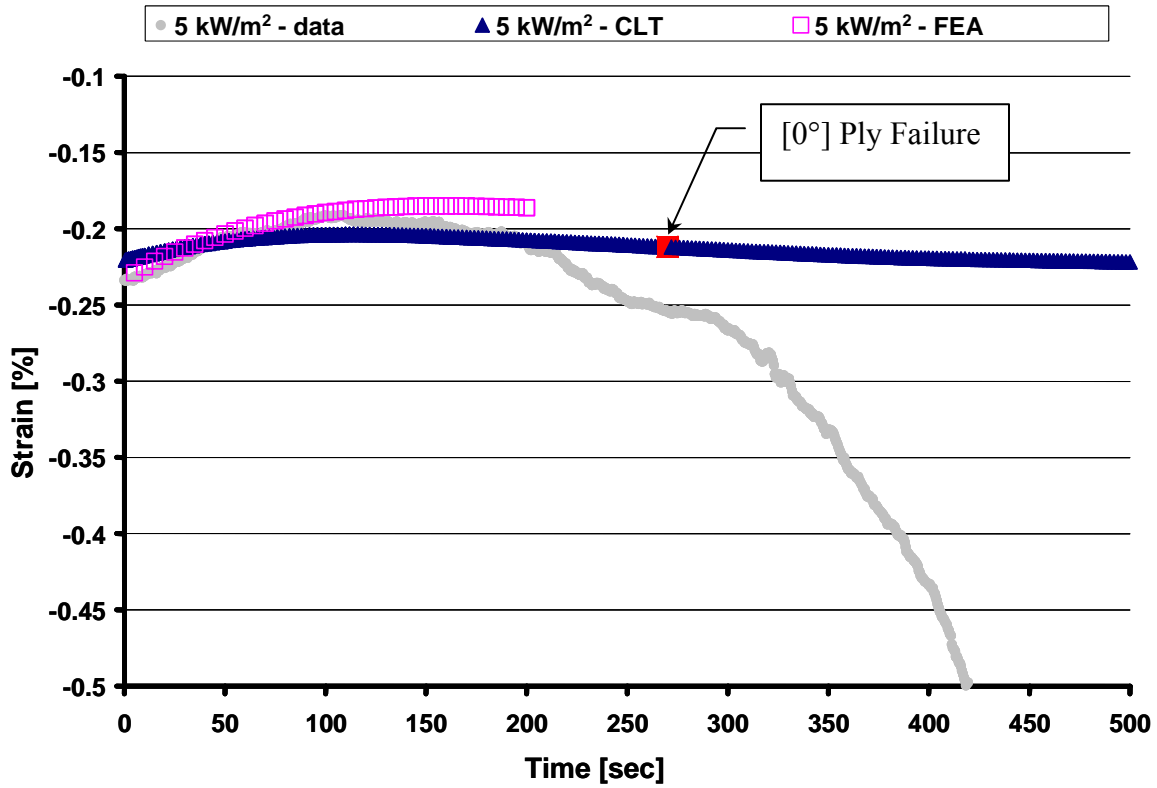


Figure 5-10: 5 kW/m²/44.8 MPa Strain Profile Predictions vs. Experimental Data

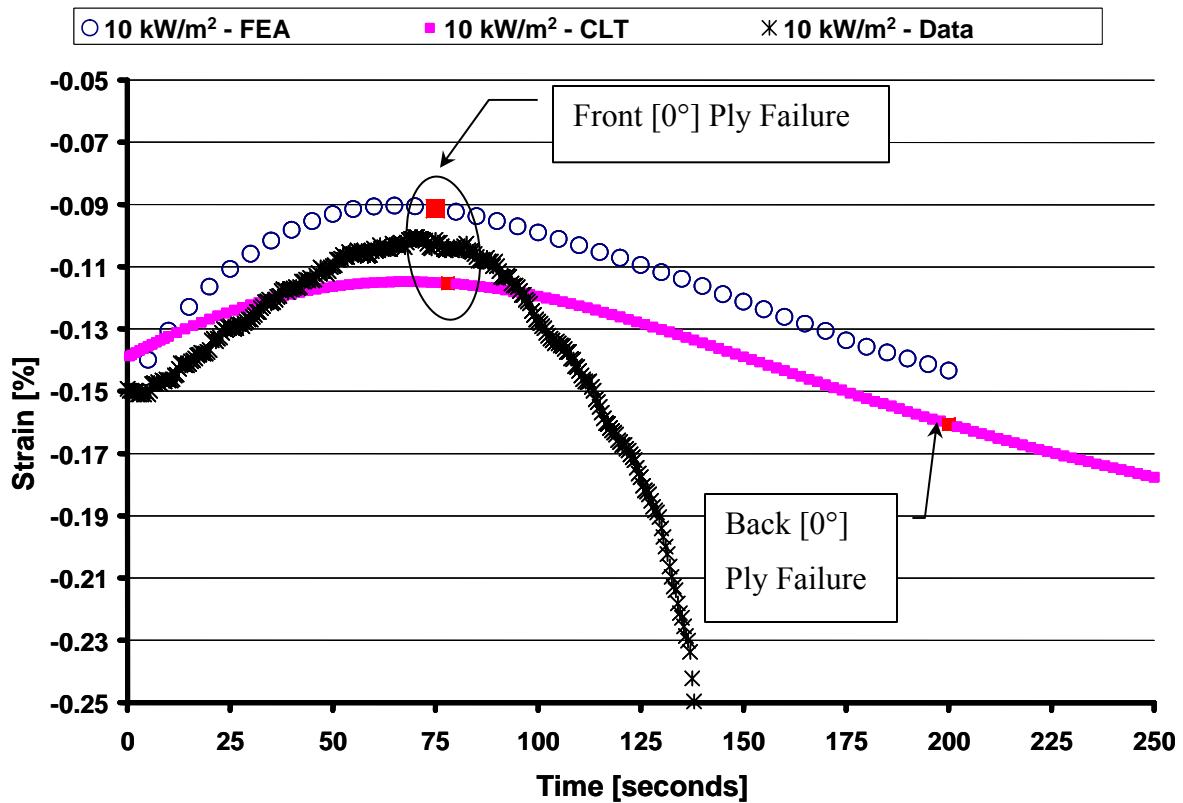


Figure 5-11: 10 kW/m²/27.6 MPa Strain Profile Predictions vs. Experimental Data

